Review

Two-Dimensional Material-Based Electrochemical Sensors/Biosensors for Food Safety and Biomolecular Detection

Tao Li [1], Dawei Shang [2], Shouwu Gao [3], Bo Wang [4], Hao Kong [5], Guozheng Yang [5], Weidong Shu [4], Peilong Xu [3] and Gang Wei [5,*

[1] College of Textile & Clothing, Qingdao University, No. 308 Ningxia Road, Qingdao 266071, China; lishilitao@qdu.edu.cn

[2] Qingdao Product Quality Testing Research Institute, No. 173 Shenzhen Road, Qingdao 266101, China; shangdawei@outlook.com

[3] State Key Laboratory, Qingdao University, No. 308 Ningxia Road, Qingdao 266071, China; qdgsw@126.com (S.G.); xpl@qdu.edu.cn (P.X.)

[4] Qingdao Institute of Textile Fiber Inspection, No. 173 Shenzhen Road, Qingdao 266101, China; wangduanyangkingpo@outlook.com (B.W.); swdqd0532@outlook.com (W.S.)

[5] College of Chemistry and Chemical Engineering, Qingdao University, No. 308 Ningxia Road, Qingdao 266071, China; konghao5@outlook.com (H.K.); yangguozheng123@outlook.com (G.Y.)

* Correspondence: weigroup@qdu.edu.cn; Tel.: +86-150-6624-2101

Abstract: Two-dimensional materials (2DMs) exhibited great potential for applications in materials science, energy storage, environmental science, biomedicine, sensors/biosensors, and others due to their unique physical, chemical, and biological properties. In this review, we present recent advances in the fabrication of 2DM-based electrochemical sensors and biosensors for applications in food safety and biomolecular detection that are related to human health. For this aim, firstly, we introduced the bottom-up and top-down synthesis methods of various 2DMs, such as graphene, transition metal oxides, transition metal dichalcogenides, MXenes, and several other graphene-like materials, and then we demonstrated the structure and surface chemistry of these 2DMs, which play a crucial role in the functionalization of 2DMs and subsequent composition with other nanoscale building blocks such as nanoparticles, biomolecules, and polymers. Then, the 2DM-based electrochemical sensors/biosensors for the detection of nitrite, heavy metal ions, antibiotics, and pesticides in foods and drinks are introduced. Meanwhile, the 2DM-based sensors for the determination and monitoring of key small molecules that are related to diseases and human health are presented and commented on. We believe that this review will be helpful for promoting 2DMs to construct novel electronic sensors and nanodevices for food safety and health monitoring.

Keywords: two-dimensional materials; nanohybrids; electrochemical sensors; biosensors; food safety; biomolecular detection

1. Introduction

With the development of modern technology and society, people pay more and more attention to their own health and environmental protection issues. It is very important to detect and monitor pathogenic factors and environmental pollutants in real-time. Among the potential detection methods, electrochemical detection has attracted the interest of researchers. The core of electrochemical detection technology is an electrochemical sensor, in which the interaction between the substance to be tested and the sensitive nanomaterial produces electrochemically active substances, and the electrochemical sensor performs qualitative and quantitative analysis by converting these substances into electrical signals [1,2]. Electrochemical sensors have been widely used in food analysis, clinical detection, environmental monitoring, and many other fields due to their simple equipment, low cost, strong response signal, good selectivity, and high sensitivity [3–5].

According to different response signals, electrochemical sensors can be divided into the current-type, potential-type, and resistance-type sensors [6]. In addition, electrochemical sensors can be divided into semiconductor sensors, light sensors, thermal sensors, field-effect sensors, etc., according to the different detection signals of the converters. The different substances detected by sensors can be divided into gas sensors, ion sensors, biosensors, etc. Compared with traditional sensors, electrochemical sensors can sense materials without destroying the surrounding system, which has obvious advantages for real-time monitoring of analytes.

In recent years, nanomaterials have developed rapidly in many fields due to their excellent electrical, magnetic, thermal, and optical properties [7–10], especially in the field of electrochemical detection, which is often used in the conversion element or induction of electrochemical sensors to improve the sensitivity and detection limit of electrochemical sensors for target analytes [11–13]. Combining nanomaterials with electrochemical sensors and utilizing the characteristics of nanomaterials can improve the detection sensitivity of the sensors, shorten the detection time, and further stabilize the physical and chemical properties of the sensors, making the detection performance of the sensors improved significantly. Among those nanomaterials, two-dimensional materials (2DMs) have become a good choice for electrode materials and attracted widespread attention in the field of electrochemistry due to their high mechanical flexibility, large specific surface area, many active sites, good chemical stability, high electrical conductivity, and thermal conductivity [14–16]. Especially the excellent heterogeneous electron transfer ability, large specific surface area, and good adsorption capacity of 2DMs make them have great application potential in electrochemical sensing [17–19].

2DMs that are currently used to fabricate electrochemical sensors mainly include graphene and its chemical derivatives [20], transition metal dichalcogenides (TMDs) [21–23], transition metal–carbon/nitrides (MXenes), metal–organic frameworks (MOFs), and others [24,25]. However, the preparation of 2DMs still faces many difficulties and challenges; the lamellar structure is especially prone to aggregation, which affects the properties of the materials and limits their wide application. Therefore, rationally designing and developing high-performance 2DMs is highly necessary in order to improve their electrochemical activity and electrode surface electrochemical signals by element doping, functionalized compounding, surface modification, and sheet thickness control of 2DMs. Meanwhile, these efforts are helpful in improving the transmission efficiency and enhance the detection sensitivity and detection speed, showing increasing application potential in electrochemical sensors and biosensors.

In this article, we present recent advances in the preparation, functional modification, and electrochemical sensor applications of 2DMs. The current preparation methods of 2DMs are based on graphene, TMOs, TMDs, MXenes, and their composites, as well as their applications in electrochemical sensors and biosensors, especially in the detection of small biological molecules, antibiotics, and pesticides, are introduced systematically. Finally, the application prospects of 2DM-based electrochemical sensors in food analysis, clinical detection, environmental monitoring, and other fields are summarized. We believe that this work will be helpful for readers to understand the design and fabrication of various 2DM-based electrochemical sensors and biosensors, which will inspire the development of sensors/biosensors for high-performance monitoring of food and environmental safety.

2. Preparation of 2DMs

Different preparation methods greatly affect the properties of the obtained 2DMs, thereby affecting their applications in electrochemical sensing. In general, the preparation methods of 2DMs can be divided into two categories: Top-down methods and bottom-up methods, as shown in Figure 1 [26]. The top-down methods can usually prepare 2DMs by exfoliating layered bulk crystals into single-layer or multi-layer nanosheets by mechanical or chemical methods, mainly including mechanical exfoliation, chemical or electrochemical exfoliation, and liquid-phase exfoliation. The mechanical exfoliation method is derived from the "scotch tape method" of graphene, in which thin layers of graphene or TMD are

exfoliated with tape and deposited onto the desired surface [27]. The thickness of 2DM nanosheets obtained by this method is difficult to control, and the yield is low, which limits the large-scale production of 2DMs. However, this method does not use any chemical substances, and the obtained materials maintain structural integrity and high crystallinity. In addition, the created 2DMs have good electronic and physical qualities, which are highly sensitive to environmental disturbances, and are very suitable as the candidates for the fabrication of electronic sensors [28–30]. For instance, Huang et al. [31] treated the substrate with oxygen plasma to remove surrounding adsorbates and introduced thermal treatment in the subsequent exfoliation process, which improved the mechanical exfoliation technique and increased the exfoliation rate and the area of the obtained graphene and $Bi_2Sr_2CaCu_2O_x$ nanosheets. This improved technique can be further used to produce other large-area 2DMs with improved yields.
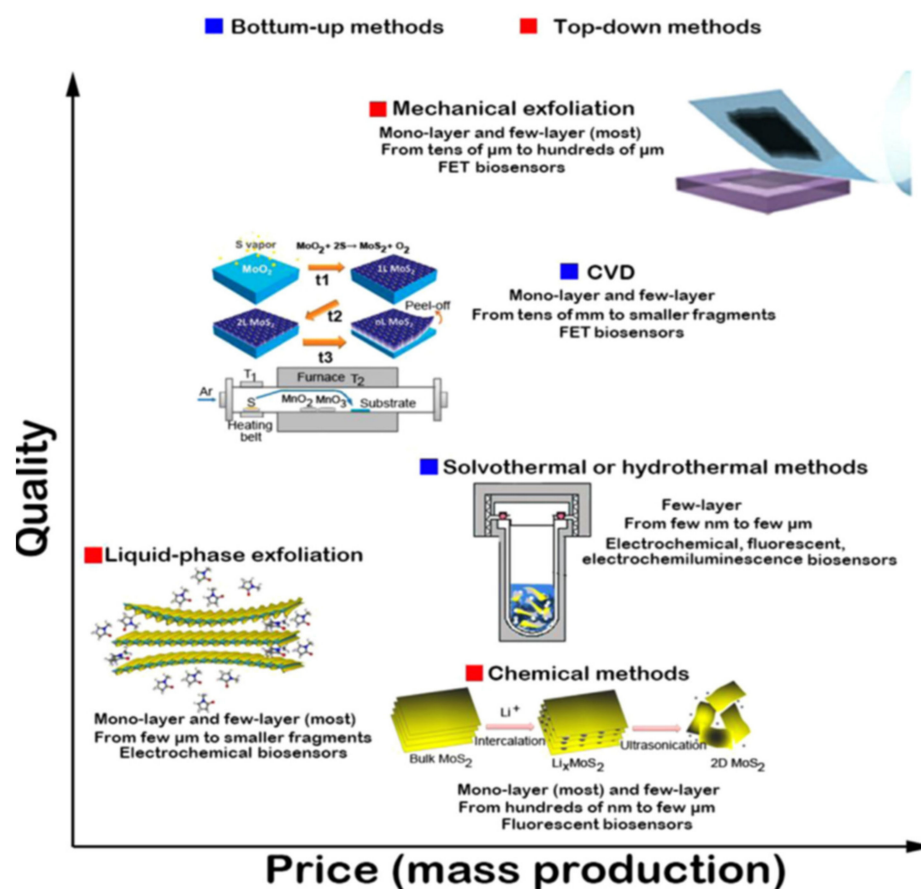

Figure 1. Several synthesis methods of mass-production of 2D MoS_2, their characteristic size and thickness distributions of the resultant 2D MoS_2, and correspondingly typical electrochemical biosensor application. Reprinted with permission from Ref. [26].

Until now, liquid exfoliation has been shown to be an alternative method for large-scale production of 2DMs [32,33]. During this process, the layered bulk crystals undergo external perturbations (such as ultrasonic waves or mechanical shocks) in the solvent to expand the interlayer spacing, resulting in the final exfoliation of the material into ultrathin 2DMs. If the right solvent can be chosen, this approach works for any layered material held together by relatively weak Van der Waals bonds. The exfoliated nanosheets were stabilized against re-aggregation in a suitable solvent, whereas re-aggregation and precipitation occurred in an unsuitable solvent. In general, a suitable solvent must satisfy the following two conditions: first, it must be able to exfoliate the 2DMs at the highest concentration possible effectively; second, it can make the resulting 2DMs stable for the longest duration. For example, Zhang et al. [34] demonstrated that ultrasonic exfoliation of WS_2, MoS_2, and BN

2D layered nanomaterials in a mixed solution of ethanol and water and the obtained 2DM nanosheet suspension has high stability. This method is simple in process and low in cost, and it can be used to prepare ultra-thin 2DMs in large quantities, and additional dispersants or intercalating agents can be introduced into the system so that the functionalized 2DMs obtained in the exfoliation process can be obtained.

The chemical exfoliation method is usually based on ion intercalation (such as Li^+), allowing other ions to enter the middle of the layered bulk crystal to expand the interlayer spacing, thereby weakening the Van der Waals interaction between adjacent layers of the bulk crystal, under mechanical vibration and ultrasonic treatment. Under the action of mechanical force, the bulky compound can be easily exfoliated into single-layer or multi-layer nanosheets. For example, Zhang et al. [14] developed an electrochemical Li^+ intercalation-assisted liquid exfoliation method by adding layered bulk crystalline materials such as MoS_2, WS_2, TiS_2, TaS_2, ZrS_2, or graphite as the cathode in the electrochemical cell. In this case, lithium foil was used as an anode, and during discharge, Li^+ ions were driven into layered bulk crystals by electrochemical force and lithium foil to form lithium intercalation compounds. The coated electrodes covered with lithium intercalation compounds were subsequently removed, washed in water or ethanol, and sonicated to obtain nanosheet suspensions. After purification by centrifugation, single-layer or multi-layer nanosheets can be obtained with a high yield. This method easily leads to defects and structural deformation and is not suitable for studying the physicochemical properties of 2DMs; however, it is beneficial for the efficient production of monolayer MoS_2 for the construction of fluorescent sensors and biosensors.

The top-down approach is only applicable to layered compound crystalline materials with limited use, while the bottom-up approach is more general, and all 2DMs can be prepared by this approach. The techniques for the bottom-up growth of 2DMs mainly include chemical vapor deposition (CVD) and solvothermal methods (also known as hydrothermal methods). The CVD technique means that the precursors containing the elements present in the 2DMs are thermally evaporated, introduced into the reaction chamber through the gas flow, and chemically reacted on the surface of a specific substrate to form the desired layered nanomaterials under appropriate reaction conditions [35–37]. For example, during the growth of MoS_2 nanosheets, MoO_3 and S powders are placed in a tube furnace with substrates such as SiO_2 or sapphire and heated to about 800 °C. The vapor formed by the evaporated powder reacts on the surface of SiO_2 to form layered MoS_2, and the thickness of which depends on the growth parameters such as the flow rate of the carrier gas and the number of reactants [38]. Thus far, CVD has been successfully used to prepare many ultrathin 2DMs, including graphene, TMD (MoS_2, WS_2, $MoSe_2$, Wse_2, etc.), metal oxides (MOs), and others [39–42]. CVD technique enables the controlled growth of 2DMs with layer number, crystallinity, and lateral dimensions on different substrates with different precursors. However, the technology generally requires high temperature and high cost of inert gas and also requires specific substrates for transfer.

The solvothermal synthesis is a simple, low-cost, and high-yield method for the preparation of ultrathin 2DMs, which can be easily dispersed in organic or aqueous media for various applications [43]. Usually, the precursor solution is put into a high-pressure reactor, hydrothermally reacted under high temperature and high pressure, and then the nanomaterials are prepared by post-processing methods such as separation, washing, and drying. For example, Xie et al. [44] prepared defect-rich multilayer MoS_2 nanosheets by the solvothermal method in the presence of excess thiourea. Dong et al. [45] prepared 2D Fe-doped NiO nanosheets with grain boundary defects using a solvothermal method through a thermally driven transformation process. The synthesized 2DMs were applied to electrocatalytic hydrogen evolution reactions. Won et al. [46] successfully synthesized a series of 2D SnS_xSe_{2-x} nanosheets with a width of 0.20–2.00 μm and a thickness of 30–68 nm without topographical defects by a solvothermal reaction. The synthesized 2DMs have a band gap of 1.36–1.96 eV and exhibited promising applications in electronic, optoelectronic, and electrocatalytic aspects. Compared with CVD, the solvothermal method is easier

to obtain much smaller crystals with high catalytic activity, which has great potential to construct electrochemical, fluorescence, and electrochemiluminescence sensors. The biggest challenge of this technology is how to block vertical growth while allowing lateral growth.

All of the above preparation methods have their own advantages and disadvantages. The choice of the preparation method depends on the specific application scenario of 2DMs. In different application systems, the factors that need to be considered include the cost, the amount of material required, desired level of crystal quality, biocompatibility, functional modification, and the final environment in which the 2DMs are used.

3. Structure and Surface Chemistry of 2DMs

Compared with zero-dimensional (0D), one-dimensional (1D), and three-dimensional (3D) nanomaterials, most 2DMs possess a larger specific surface area, which facilitates analyte loading and thus improves the sensitivity of material-based sensors. Moreover, the relatively large lateral dimensions of 2DMs can be in close contact with electrodes and thus, have attracted extensive attention in applications, including electrochemical sensors [47–49]. Currently known 2DMs mainly include graphene and its derivatives, transition metal dichalcogenides (TMDs) represented by MoS_2, transition metal–carbon/nitrides (MXene), MOs, and others, as shown in Figure 2 [50].

Graphene family	Graphene	hBN 'white graphene'		BCN	Fluorographene	Graphene oxide
2D chalcogenides	MoS_2, WS_2, $MoSe_2$, WSe_2		Semiconducting dichalcogenides: $MoTe_2$, WTe_2, ZrS_2, $ZrSe_2$ and so on		Metallic dichalcogenides: $NbSe_2$, NbS_2, TaS_2, TiS_2, $NiSe_2$ and so on	
					Layered semiconductors: GaSe, GaTe, InSe, Bi_2Se_3 and so on	
2D oxides	Micas, BSCCO	MoO_3, WO_3	Perovskite-type: $LaNb_2O_7$, $(Ca,Sr)_2Nb_3O_{10}$, $Bi_4Ti_3O_{12}$, $Ca_2Ta_2TiO_{10}$ and so on		Hydroxides: $Ni(OH)_2$, $Eu(OH)_2$ and so on	
	Layered Cu oxides	TiO_2, MnO_2, V_2O_5, TaO_3, RuO_2 and so on			Others	

Figure 2. Current 2DMs. The color blue indicates the stable monolayers under ambient conditions, green indicates those probably stable in air, and pink indicates those unstable in the air but may be stable in an inert atmosphere. Grey indicates monolayers exfoliated by 3D compounds, and "Others" indicates 2D crystals, including borides, carbides, and nitrides [50].

3.1. Graphene

Graphene is a honeycomb-like 2D structure composed of a single layer of sp^2 carbon atoms, which is the basic building block of other carbon-based allotropes, such as graphite, carbon nanotubes, and fullerenes [51]. Graphene has many excellent properties, such as high transparency (97.7% visible light transmittance), high thermal conductivity (3×10^3–5×10^3 W m^{-1}K^{-1}), electrical conductivity (10^4 Ω^{-1}) at room temperature, high Young's modulus (130.5 GPa), and high specific surface area (2630 m^{2}g^{-1}) [52–54]. In addition, graphene also has a special π-π* energy band structure, in which carbon atoms form a single-layer honeycomb lattice through sp^2 hybridization, and its bandgap and conductivity are related to the number of layers and approach the bandgap and conductivity of graphite with the increase in the number of layers [55]. These unique structures provide it with excellent electrochemical performance while also showing excellent performance in many fields such as optical and biomedical disciplines.

Due to its large specific surface area, high electrical conductivity, abundant surface atoms, high mechanical strength, and potential for large-scale production, graphene has shown great potential in the field of electrochemical sensing [56,57]. First, graphene exhibits remarkably high carrier mobility and density at room temperature, which make it a good material for the construction of high-performance electrical devices [58,59]. Second, the graphene surface can interact with various analytes through Van der Waals forces, electron

transfer, and covalent bonds, which lead to changes in graphene electronic properties, especially electrical conductivity [60,61]. The electron density inside graphene-based materials can be concentrated at its edges and structural defects, resulting in faster electron transfer rates than in the substrate plane, demonstrating the versatile properties of graphene as an electrocatalyst for electrochemical sensing applications [62]. Third, graphene has a high specific surface area, where each carbon atom is a surface atom, providing the largest surface area per unit volume, so charge transport through graphene is very sensitive to its chemical environment [63,64]. Fourth, graphene has excellent mechanical strength and flexibility, which are compatible with flexible wearable electronics [65,66]. The above-mentioned unique properties make graphene the most promising 2DM system in the field of electrochemical sensors.

Since the graphene surface plays a crucial role in intermolecular interactions, tuning the surface chemistry of graphene materials is the most important and direct way to tune their sensing performance. In order to enhance the interaction with the surrounding environment, the graphene surface is usually modified by various doping. The sensing performance in electrochemical sensing devices can be enhanced by incorporating functional groups or dopants after synthesis, as well as achieving structural and defect control and tuning the reactive sites of adsorbed chemicals. Compared with pristine graphene, graphene oxide (GO)-based gas sensors with defects and oxygen-containing functional groups have higher selectivity and sensitivity [67–69]. In addition, graphene materials can also be combined with other functional nanomaterials (such as metal nanoparticles [70], MO nanoparticles [71], conductive polymers [72], etc.) to form heterostructures, and the sensing properties can be further improved through the synergistic effect of different components. For example, the modification of graphene with conducting polymers can enhance the carrier scattering of graphene to form adsorbent layers that provide electrochemical interactions with a range of molecules [73], while the modification of enzymes can induce selectivity for biomolecules [74]. Combining graphene and MO for gas sensors can reduce the gas detection temperature and improve the sensitivity and response/recovery speed [75,76]. When applying graphene to electrochemical sensors, the effects of surface modification, lattice defects, and electronic properties on different surface chemical reactions should be considered.

3.2. TMDs

Two-dimensional TMDs have been favored by researchers due to their atomically thin structures and excellent electrical properties [77]. TMDs have a true 2D structure, but the physical properties are quite different from graphene. The monolithic form of TMDs has a layered structure of X-M-X, in which transition metal atoms (M) are sandwiched between two layers of chalcogen atoms, X, in a stoichiometric ratio of MX_2. A common feature of these materials is that atoms in the same layer are covalently bonded into hexagons, and weak Van der Waals forces exist between adjacent layers, making stacking or thinning prone to occur [78,79]. TMDs can display a wide range of polymorphisms [80–82]. For example, MoS_2 has four different crystal structures, namely 2H, 1T, 1T', and 3R, depending on the coordination pattern between Mo and S atoms and the stacking order between layers [83]. The electrical conductivity of bulk TMDs also has various characteristics ranging from insulator (HfS_2) to semiconductor (MoS_2) and conductor (NbS_2). The electronic properties of TMDs are significantly different from the bulk properties due to the fracture of the interlayer coupling [84,85]. When TMDs are exfoliated into 2D nanosheets, both basal planes and prism edges are exposed, exhibiting distinct structural and electronic properties. The basal surface of TMDs is mainly composed of chalcogenides, and on the edges of the prisms, metal or chalcogen atoms exist [41].

The advantages of TMDs, such as high thermal/chemical stability and abundant metal sites, make these 2DMs promising candidates for electrochemical sensing applications [86]. For example, the increased bandgap of MoS_2 after exfoliation from bulk materials into nanosheets makes it an excellent choice for fabricating electronic devices [87]. The phase

transition of MoS_2 makes its transition from a semiconducting material to a metallic material, which enhances its electronic conductivity, and further optimizes its electrochemical properties [88,89]. In addition, the single-layer TMD nanosheets have a huge surface area, which enables their surfaces to adsorb biomolecules in large quantities. At the same time, 2D TMD nanosheets exhibit a very superior fluorescence quenching ability for fluorescent molecules, which also makes these materials have great potential in the construction of fluorescent biosensors [90,91].

The representative substances of TMDs include MoS_2, SnS, and SnS_2, among which MoS_2 is the most widely studied one. Monolayer MoS_2 is a semiconductor with a direct bandgap of 1.8 eV and a high absorption coefficient to generate efficient electron–hole pairs. This property largely compensates for the shortcomings of graphene (zero bandgaps), thereby broadening the application of 2DMs to ultrasensitive optoelectronic devices [92]. In addition, monolayer MoS_2 has electron mobility >200 $cm^2V^{-1}s^{-1}$ at room temperature, high current on/off ratio (1×10^8), and high carrier lifetime (100 ps), which are suitable for use as a field-effect or electrochemical biosensor [93]. More importantly, the ultrathin planar structure of MoS_2 confines the electrons/holes in the plane of atomic thickness, making it sensitive to the surrounding environment, and the edges can be terminated with Mo or S atoms by processing. This tunable electronic energy state makes it a promising substrate material for the construction of electrochemical sensors, offering great potential for various applications (Figure 3).
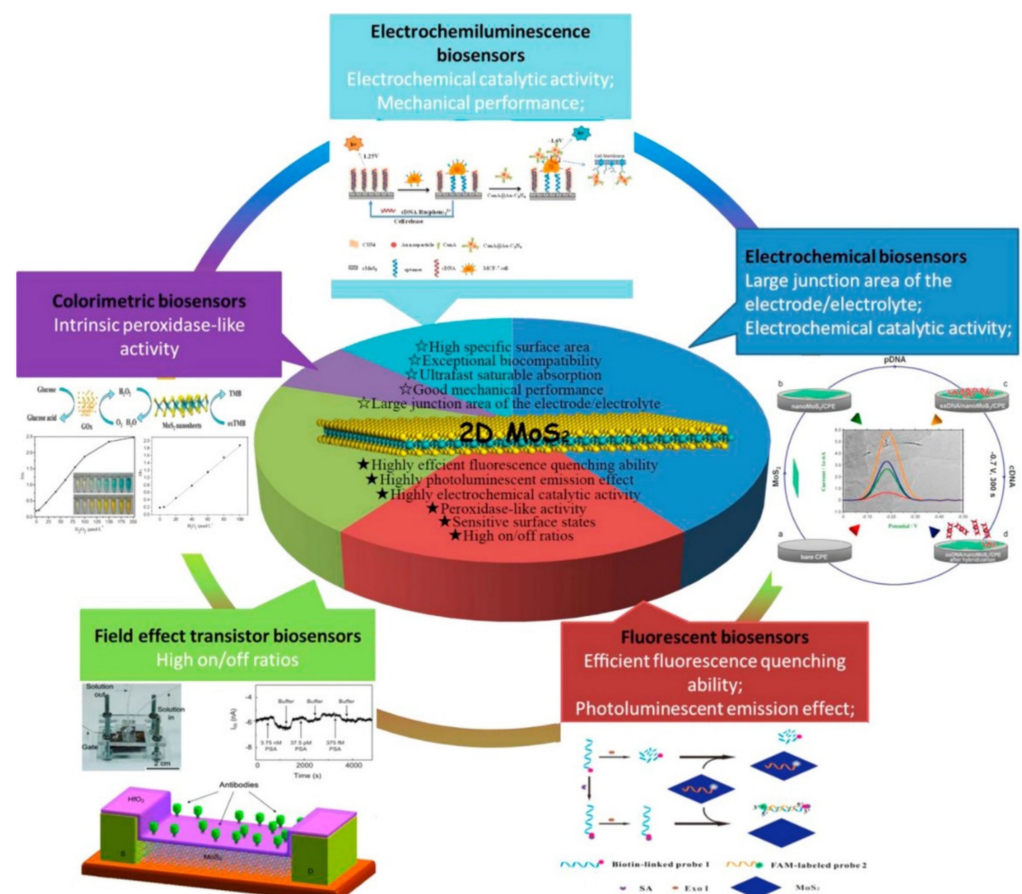

Figure 3. Intrinsic properties of 2D MoS_2 and most representative properties applied in a specific biosensor. Reprinted with permission from Ref. [26].

Theoretical calculation showed that MoS_2 containing S vacancies had good adsorption capacity for several non-polar gases, while perfect MoS_2 sheets had little or no adsorption for several non-polar gases [94]. The location and number of S vacancies at the edge of MoS_2 nanosheets also have important effects on their stability and catalytic activity [95]. The S

vacancies in MoS$_2$ are most likely to form at the edges or corners of the nanosheets, and their specific locations/distributions depend on the size of the 2D nanosheets. Therefore, it is important to control the specific shapes of TMD nanosheets (hexagonal sheets, lamellar crystals, triangular sheets, etc.) in terms of morphology and size [96,97]. For small-sized MoS$_2$ nanosheets, the shape can be engineered by the functionalization of the edge plane since the equilibrium geometry is highly sensitive to the energy of the edge atoms [98]. This molecular-level control enables great tunability of the electrochemical reactions and electronic properties of 2D TMD nanosheets, which can be applied in sensing technologies.

Although, MoS$_2$ has many advantages, such as a suitable bandgap and large specific surface area, extraordinary biocompatibility, and easy functionalization. However, due to the dependence of Van der Waals interaction between the atomic layers of MoS$_2$ [99], the conductivity tends to be low in the application process, and it is prone to agglomeration, which inhibits the electron transfer ability [100]. Therefore, it is necessary to compound some highly conductive materials (such as metal nanoparticles, carbon materials, conductive polymers, graphene, etc.) to solve this problem and make it better applied to sensor electrode materials [101–103]. The composition of 2D MoS$_2$ with nanoparticles such as metals not only retains the advantages of large surface area and abundant active sites of 2D MoS$_2$ but also improves the electrical conductivity. The synergistic effect produced by the combination of the two components can obtain nanocomposite materials with superior performance, which produces good results in electrochemical sensors. For example, Wang et al. [104] successfully combined 2D MoS$_2$ and Au and used Ag nanospheres as a marker to detect carcinoembryonic antigen. Yagati et al. [105] prepared Au-MoS$_2$ composites on indium tin oxide (ITO) substrates by electrodeposition and used them for the detection of T$_3$ in clinical serum with good results.

Since graphene has a similar microstructure and morphology to MoS$_2$, it can be used as an ideal substrate for the growth of MoS$_2$ nanosheets. The addition of graphene not only greatly improves the electrical conductivity but also promotes the formation of MoS$_2$ nanosheets on graphene. The MoS$_2$/graphene composites prepared by different methods have been shown to have good electrical conductivity and electrochemical performance in electrochemical sensors, which can measure antibiotics, ascorbic acid, dopamine, and uric acid [106–108].

3.3. TMOs

TMOs are compounds formed from metals and oxygen in the form of oxide ions and are the most diverse class of solids with various structures and properties. According to the existence of Van der Waals layered structure in the bulk, 2D TMOs can be divided into two categories: 2D layered TMOs (such as MoO$_3$, TaO$_3$, WO$_3$, etc.) and 2D non-layered TMOs (ZnO, CuO, and SnO$_2$ nanosheets or nanofilms, etc.) [48,109–111]. For example, orthorhombic MoO$_3$ is a typical layered structure in which bilayer planar crystals of MoO$_6$ octahedra are held together by Van der Waals forces in the vertical direction [112]. The weak interactions between these layers facilitate exfoliation by liquid or gas phase techniques to obtain nanosheets. Different TMOs have different electronic properties, and their electrical conductivities vary from metals to insulators. The conductivity of specific TMOs can be further tuned by changing crystal size, morphology, dopants, geometry, and temperature [113].

The ionic nature of oxygen ions and metal–oxygen bonds are two key factors that determine the surface properties of TMOs [114]. The unique properties of oxygen ions determine the performance of 2D TMOs in electrochemical sensings, such as molecular adsorption, charge transfer, and catalytic performance [115,116]. Specific energy states near or on the surface of 2D TMOs can generate Coulomb interactions with neighboring ions. Therefore, if the surfaces of two TMOs come into contact with each other, an interfacial potential is created, which changes the Fermi level of the surfaces [117]. Due to the strong ionic nature of TMOs, the surfaces of 2D TMOs can be electronically activated to enable various small molecules to adsorb on their surfaces. For example, at room temperature,

oxygen is usually adsorbed on the surface of 2D TMOs in the form of negatively charged compounds [118]. The basal planes of layered MOs are terminated by oxygen atoms and have high chemical stability in air and water.

TMOs have been widely used in electrochemical sensors due to their semiconducting properties. At high temperatures (T > 250 °C), atmospheric oxygen increases the hole carrier concentration by binding to oxygen vacancies on the surface of MOs, enabling these materials to obtain stronger electrical conductivity at high temperatures [119,120]. However, the application of TMOs in sensing requires high operating temperatures, which consume a large amount of electricity relative to sensors that can operate at room temperature [121]. At the same time, due to the high working temperature, it has extremely high requirements for the environment and conditions of use, which greatly affects the service life and restricts the application range of TMOs sensors. In order to solve this problem, the sensing properties of materials are usually improved by doping or compounding with other semiconductor materials by using their synergistic effects [122–124]. For example, Xu et al. [125] used theoretical calculations to study the sensitivity of In-doped ZnO nanosheets to acetylene gas. It was found that the incorporation of In atoms into the ZnO nanosheets increased the adsorption energy of acetylene from -3.6 kcal/mol to -20.4 kcal/mol due to cationic interactions. In the presence of O_2, H_2O, N_2, and CO_2, the In-doped ZnO sheet can selectively detect acetylene gas with a short recovery time and high sensitivity. In another case, Zhou et al. [126] prepared NiO/ZnO nanosheets by a one-step hydrothermal method and examined their gas-sensing properties towards SO_2. It was found that at the optimal operating temperature of 240 °C, the NiO/ZnO nanosheet-based sensor device had a response of 28.57 to 50 ppm SO_2 and a gas detection range of 5–800 ppm.

3.4. Transition Metal–Carbons/Nitrides (MXene)

MXene is a new 2D transition metal–carbon/nitride with a structure similar to graphene [127–129]. In 2011, Naguib et al. [130] used concentrated hydrofluoric acid (HF) to selectively etch the Al atomic layer in the ternary layered cermet material Ti_3AlC_2 and successfully synthesized Ti_3C_2 nanosheets with layered morphology. A large number of functional groups, such as -OH, -F, and =O, are formed on the surface of MXene during the preparation process, giving it a unique structure, excellent electrical conductivity, and excellent properties such as environmental protection, which stimulates great enthusiasm for research and exploration [131].

MXene is generally prepared by selective etching of its precursor MAX phase with concentrated hydrofluoric acid [132,133]. The MAX phase is a cermet material with a unique ternary layered structure, and its general formula is $M_{n+1}AX_n$, where M is a transition metal element, A is a group III or group IV main group element (mainly Al or Si), X is C and/or N elements, $1 \leq n \leq 3$ [134]. In the MAX phase, there is a metallic bond between the M atom and A atom, while a mixed bond with a stronger binding force between the M atom and X atom mainly includes covalent, ionic, and metallic bonds. Therefore, it is possible to make use of the different bond energies between M-X and M-A to break the weaker M-A bond through some specific methods without destroying the M-X bond, thereby removing the A atomic layer and preparing a lamellar structure $M_{n+1}X_n$. According to the difference of n, there are mainly three structures 211, 312, and 413 (Figure 4) [135]. The MXene materials that have been successfully synthesized so far include Ti_3C_2, Ti_2C, V_2C, Ta_4C_3, $(V_{0.5}Cr_{0.5})_3C_2$, and $(Ti_{0.5}Nb_{0.5})_2C$, etc. [136,137]. Among them, Ti_3C_2 is the most studied 2DM among MXene materials.
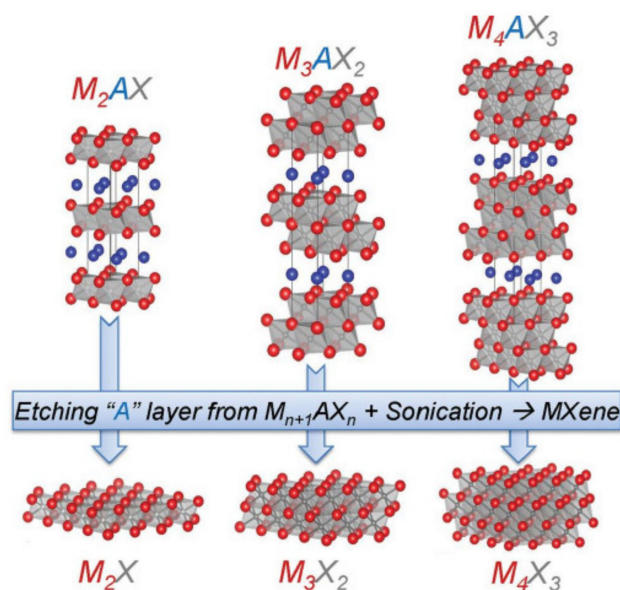
Figure 4. Schematic diagram of the structure of MXene and its corresponding MAX phase. Reprinted with permission from Ref. [135].

The surface activity of MXene prepared by the liquid etching method is extremely high, and it can rapidly react with water, fluoride ion, and oxygen in the solution to reduce the energy of the whole system. Therefore, MXene surfaces generally contain functional groups such as -OH, -F, and =O, and these functional groups are generally located in the most stable symmetrical positions in the MXene lattice structure [138,139]. By changing the surface functional groups, MXene materials can be switched between conductors and semiconductors. Theoretical calculations showed that after etching the A atomic layer in the MAX phase, the d-orbital electrons of the M atoms are rearranged, resulting in the metallic conductivity of the MXene nanosheet materials [140]. When the surface of the MXene nanosheet is occupied by functional groups such as -OH and -F, its band structure again exhibits semiconducting properties [130]. Mauchamp et al. [141] used high-resolution electron energy loss spectroscopy to study the properties of MXene materials and found that the surface plasmons could be tuned in the mid-infrared band of 0.2~0.7 eV by controlling the surface functional groups and thickness of MXene materials. In another study, Pellegrini et al. [142] found that plasmons can be used to enhance the performance of mid-infrared light sources, sensors, and detectors for chemical sensing and thermal imaging.

As 2D nanosheet materials, Mxene materials have more abundant elemental composition and complex mixed bonds than graphene materials. Therefore, MXene materials have more potential for modification towards specific applications. In order to improve the properties of MXene materials, other nanomaterials are combined with MXene to improve their original properties through synergic effects, thereby greatly improving the selectivity and sensitivity of MXene-based electrochemical sensors [143,144]. For example, Wang et al. [145] prepared TiO_2-Ti_3C_2 nanocomposites based on Ti_3C_2 and used the created materials to immobilize hemoglobin (Hb) to construct a mediator-free hydrogen peroxide (H_2O_2) sensor with high stability and low detection limit. The experimental results showed that the TiO_2-Ti_3C_2 nanocomposites had good biocompatibility with Hb and provided excellent protein biological activity and stability. The detection range was 0.1~380 μM with a detection limit of 14 nM. Meanwhile, the fabricated sensor could maintain 94.6% of the performance after 60 days.

3.5. Other 2DMs (BPs, C₃N₄, MOFs, 2D Polymers, and Others)

Black phosphorus (BP), as an emerging 2D material, represents high carrier mobility and a tunable mild direct bandgap, which can be applied in the fields of electronics and optoelectronics. Two-dimensional BP is a single-layered crystal material composed of sp^3 hybridized phosphorus atoms arranged in a layered orthorhombic structure with the space group [146]. BP has a distinctly nonplanar honeycomb lattice structure with lattice constants a = 3.31, b = 10.50, c = 4.38 Å [147]. BP also shows a folded conformation along with the armchair orientation, with the bilayer structure along the zigzag orientation predominant (Figure 5a) [148]. The folded structure creates unique intrinsic anisotropy, resulting in excellent exploitable electronic, optical, thermal, and mechanical properties. In addition, the biocompatibility of BP is very beneficial for biomedical applications. Similar to graphene, BP single crystals are bound by the Van der Waals forces and consist of vertically stacked and weakly crystalline layers with a distance of 5.5 Å from adjacent layers (Figure 5b). In each phosphorus layer, the P atoms exhibit a triangular pyramid structure due to the covalent bonding of phosphorus atoms with one lone electron pair, and defects may exist in the monolayer due to the loss of P atoms (Figure 5c), which favors the dissociation of the thin layer of black phosphorus atoms [148]. The mass production of BP thin layers is still in its infancy, and mechanical and liquid phase exfoliation are one of the most effective methods to obtain high-quality flake BP [149,150]. For example. Castellanos-Gomez et al. [151] used viscoelastic polydimethylsiloxane (PDMS) to exfoliate BP flakes after tape peeling, optimizing the peeling process, increasing the yield, and reducing the tape contamination. Brent et al. [150] performed liquid-phase exfoliation of BP in N-methylpyrrolidone (NMP), sonicated and centrifuged to obtain 3~5 layers of high-purity BP nanosheets (200×200 nm²). Zhao et al. [152] replaced traditional organic solvents with eco-friendly ionic liquids to prepare BP nanosheets, and the high-concentrated dispersions (0.95 mg mL^{-1}) were stable in the environment for more than a month.

The rapid development of BP-based gas/small molecule sensors has stimulated applications in biomolecule detection due to their superior sensing performance [153]. For instance, Chen et al. [154] prepared a BP-based FET biosensor for sensitive detection of antigen–antibody interactions. The mechanically exfoliated layered BP was passivated by Al_2O_3 to form the sensing/conducting channel of the FET, which was subsequently further modified with antibody-conjugated AuNPs. The antigen bound to the black phosphorus surface generated a negative gate potential, which changed the conductivity of the biosensor. The fabricated FET sensor could be used as a stable and rapid immunoglobulin G (IgG) diagnostic tool with a detection limit of 10 ng mL^{-1}.

g-C_3N_4, a similar graphite material, is a layered structure composed of interlayer Van der Waals force [155–157]. The crystal structure of g-C_3N_4 is generally considered to be an N-substituted graphitic phase framework structure (Figure 5d–f), which is formed by sp^2 hybridization of C and N atoms [158]. Bulk C_3N_4 can be processed by exfoliation and other methods to obtain nanoscale g-C_3N_4, such as g-C_3N_4 nanosheets, whose properties are very different from those of bulk materials. g-C_3N_4 nanosheets have good thermal and chemical stability, fluorescence effect, and other excellent properties [159–161]. g-C_3N_4 contains a small amount of hydrogen in the form of primary and/or secondary amine groups at its terminal due to incomplete condensation during the synthesis. The presence of terminal hydrogens and the high electron affinity of nitrogen for many analytes result in g-C_3N_4 with rich surface properties, including basic surface functions, electron-rich properties, and H-bond motifs [162]. The C and N elements of the g-C_3N_4 nanosheets are uniformly dispersed in each nanosheet with good thermal stability and tunable bandgap. Its excellent properties make it widely used in photocatalysis, photovoltaic power generation, bioimaging, and sensing [161].

Hexagonal boron nitride (h-BN) is another graphitic analog that has a periodic structure similar to graphene in plane, but with a different stacking order [163,164]. Adjacent layers with a distance of 3.30–3.33 Å gather together under the Van der Waals force to form bulk crystals (Figure 5g–i) [164,165]. h-BN is an electrical insulator with a bandgap

of 5.2 eV, high thermal conductivity, excellent dielectric properties, and high-temperature oxidation resistance [166,167]. Within the BN nanosheets, the chemical alternation of boron (B) and nitrogen (N) atoms results in the ionic nature of this crystal, which can be highly sensitive to various gases. The adsorption of gas molecules greatly changes the electronic properties of BN nanosheets, which is a prerequisite for the fabrication of gas sensors. In addition, 2D BN nanosheets allow all of their atoms to be exposed to adsorbed gas molecules, thereby increasing the sensitivity of the sensors. Due to its high thermal stability and chemical inertness, BN nanosheets can also be used in harsh environments where other materials cannot. According to theoretical calculations, doped or defective h-BN nanosheets can respond to several gas molecules. For example, Ma et al. [168] studied the Pd-doping behavior on the h-BN monolayer as well as related adsorption and sensing performance upon three SF_6 decomposed species to explore its sensing potential. They found that the adsorption performance of Pd–BN monolayer upon SF6 decomposed species is in order as SOF_2 > SO_2 > SO_2F_2. After gas adsorption, the bandgap of the Pd–BN monolayer is remarkably changed; the sensitivity is obtained as −41.04%, −108.14%, and 2.55% for SO_2, SOF_2, and SO_2F_2 systems, respectively, which implies the superior sensing behavior upon SOF_2 at room temperature. Yamini et al. [169] investigated the electronic response of pristine and topologically defected h-BN nanosheets toward NO molecule using density functional theory calculations and found that the HOMO/LUMO gap of the pristine and Stone–Wales defected h-BN sheet is significantly decreased about 42% and 35%, respectively, upon NO adsorption which may increase the electrical conductance of the sheet and it might be potentially used in NO sensors. In addition, BC_3 nanosheets such as BN and graphene were also demonstrated to be used to fabricate electrochemical sensors as a suitable choice for Megazol detection [170].
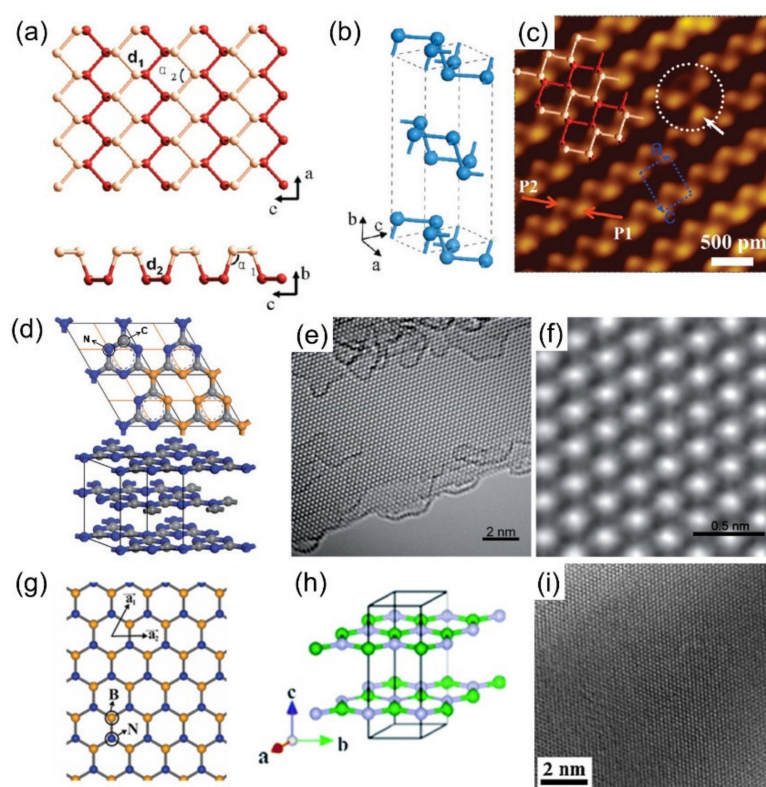

Figure 5. (**a**) Scheme of a single layer BP on the a-c and b-c plane. The upper and lower atoms are presented in pink and red, respectively. (**b**) Schematic illustration of unit cell. (**c**) High-resolution image of BP [148]. (**d**) Crystallographic unit cell and AB stacking arrangement of triazine-based g-CN layers. (**e**,**f**) HRTEM image of mechanically cleaved nanosheet of g-CN [158]. (**g**,**h**) Structure of h-BN, (**g**) The 2D floor plan; (**h**) Stereogram [164]; (**i**) HRTEM image of BN nanosheets [165].

4. Applications of 2DM-Based Electrochemical Sensors and Biosensors

4.1. 2DM-Based Electrochemical Sensors/Biosensors for Food Safety

4.1.1. Detection of Nitrite

In food safety and quality analysis, electrochemical sensors have been widely used in the detection of pesticide residues, heavy metal ions, pathogenic bacteria, and toxins. The application of a large number of inorganic fertilizers in crop cultivation greatly increases the content of nitrite in the environment. Nitrite can inhibit the growth of microorganisms in the food industry and is often used as a dye for meat products. Therefore, nitrite is very likely to enter the human body, making hemoglobin irreversibly converted into methemoglobin, which cannot exchange oxygen normally, disrupt the oxygen delivery system, and cause hypoxia. It may also lead to the production of carcinogen N-nitrosamine in the stomach. The content of nitrite in drinking water should be less than 3 mg/L [171]. Therefore, a sensitive, rapid and accurate method for the determination of nitrite is necessary. A variety of methods were used to detect the content of nitrite effectively. Compared with other methods, electrochemical sensors have attracted the attention of researchers due to their advantages, such as fast detection speed, wide linear detection range, low detection limit, and high stability [172]. 2DMs, such as MoS_2, graphene, and others, were widely used in the field of electrochemical detection because of their abundant active sites and large specific surface area [173–175].

However, the electrical conductivity of 2D MoS_2 limits its application in the field of electrochemical detection. Compounding it with metal nanoparticles can effectively improve its detection sensitivity. For example, Zhang et al. [176] prepared 2D MoS_2 by hydrothermal method and AuNPs by chemical reduction method. MoS_2/AuNPs composites were prepared by mixing the as-prepared two components and further utilized for the fabrication of electrochemical sensors. By electrochemical tests, nitrite in tap water was detected. The MoS_2/AuNPs composites-based electrochemical sensor exhibited a wide linear detection range (0.005–27.78 mM), low detection limit (1.7 μM), and good recovery rate, and the detection process is actually an oxidation process from nitrite to nitrate. In another study, Yang et al. [177] prepared 2D MoS_2 by mechanical milling and ultrasonic liquid phase peeling. MoS_2/Ni nanocomposites were prepared in situ by chemical reduction method and applied to electrochemical detection of nitrite with a wide detection range (5–800 μM) and low detection limit (2.48 μM). In addition, MoS_2/Ni-modified electrode also has excellent detection characteristics such as high stability, repeatability, anti-interference, and recovery. Haldorai et al. [178] prepared electrochemical nitrite sensors based on spindle-shaped Co_3O_4 and rGO nanocomposites with good reproducibility, high stability, high sensitivity, and high selectivity in the process of nitrite detection, as shown in Figure 6. The fabricated sensor exhibited a detection limit of 0.14 μM with a linear detection range of 1–380 μM. Zhang et al. [179] prepared the Fe_3O_4/MoS_2 nanocomposite structure of Fe_3O_4 nanospheres uniformly dispersed on MoS_2 nanosheets by hydrothermal method. Fe_3O_4/MoS_2 nanocomposites were used to modify the glassy carbon electrode (GCE) for the detection of nitrite with a wide detection range (1.0–2630 μM) and a low detection limit (0.5 μM).
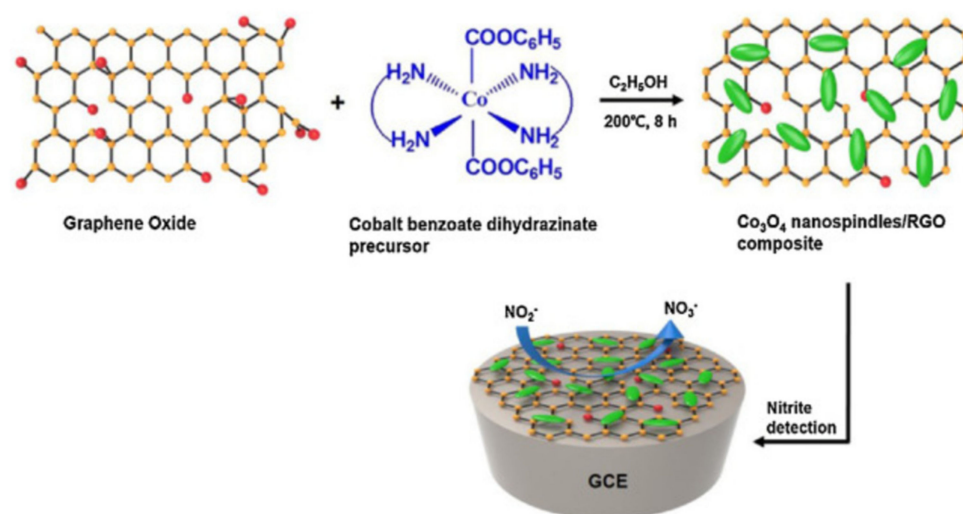
Figure 6. Schematic presentation on the fabrication of rGO and Co_3O_4-based electrochemical nitrite sensor. Reprinted with permission from Ref. [178].

4.1.2. Detection of Heavy Metal Ions

Heavy metal ions (such as Pb^{2+}, As^{3+}, Cd^{2+}, Hg^{2+}, etc.) seriously harm the ecological environment and enter the animals and plants within the food chain, and eventually endanger human health [180,181]. Therefore, it is very important to develop a highly sensitive and selective method for the detection of heavy metal ions. In recent years, the electrochemical sensor has been used in the detection of heavy metals because of its low cost, fast response time, and easy operation.

For example, Zhou et al. [182] used L-cysteine-functional graphene to fabricate an electrochemical sensor, which could simultaneously detect trace heavy metal Pb^{2+} and Cd^{2+} ions in food. Zhu et al. [183] carried out alkali intercalation treatment on the synthesized Ti_3C_2. The detection performance of Ti_3C_2 for heavy metal ions was studied by electrochemical analysis. The experimental results indicated that alkaline Ti_3C_2 has high sensitivity and a good linear relationship for the detection of heavy metal ions, and the detection limit is up to trace level.

Graphene materials are very good candidates for the fabrication of electrochemical sensors for food safety. Mahmoudian et al. [184] constructed the electrode modified by Fe_3O_4 and rGO nanocomposites. The current density on the surface of the electrode is high (~400 μ A/cm^2), and heavy metal ions such as Ag^+, Cu^{2+}, Hg^{2+}, Bi^{3+}, Cr^{2+}, Fe^{3+}, and other heavy metal ions did not interfere with the quantitative detection of Pb^{2+}. Tan et al. modified single-stranded DNA aptamers on rGO by linear sweep voltammetry to construct a highly sensitive Hg^{2+} sensor, which could eliminate the interference of other metal ions and detect Hg^{2+} ions of 0.5 nM with high selectivity so as to detect the content of Hg^{2+} ions in water conveniently, quickly, and selectively [185]. Rahman et al. [186] prepared GO and silver nanowires (Ag NWs) composite-modified Pt electrodes for the determination of Hg^{2+}. The synergistic effect of GO and conductive Ag NWs greatly promoted the electron transport and sensing ability of Hg^{2+}. The detection limit of Hg^{2+} was 0.1 nM, which is significantly lower than the safety limit set by the World Health Organization. The sensor was used for the detection of Hg^{2+} in tap water samples with excellent performance, so it could be a promising field monitoring platform for Hg^{2+} in water. Wei et al. [187] prepared SnO_2-rGO nanocomposites with uniform particle size and controllable structure under a one-step wet chemical method. Additionally, SnO_2-rGO nanocomposites were used to modify the electrode to construct electrochemical sensors. Based on the excellent catalytic activity and electron conduction ability of SnO_2-rGO, the sensor achieved highly sensitive synchronous analysis of Cd^{2+}, Pb^{2+}, Cu^{2+}, and Hg^{2+}, and the detection limits were 11.4, 38.1, 14.4, and 55.9 nM, respectively.

Sun et al. [188] prepared GO/MnO$_2$ nanocomposites by a simple synthesis method and modified GCE for electrochemical detection of Cu^{2+} and Pb^{2+}, as shown in Figure 7. It was found that MnO$_2$ was uniformly attached to the layered structure of GO, forming more adsorption sites. Under the optimum conditions, the linear range of GO/MnO$_2$/GCE for Cu^{2+} and Pb^{2+} was 0.05 to 1 µM, and the detection limits were 1.67 and 3.33 nM, respectively. Jiang et al. [189] prepared a polysulfide/graphene nanocomposite, which can be modified onto the carbon substrate using GO as the matrix and decorated with polysulfide groups, and used as an electrochemical sensing platform for highly sensitive and selective detection and analysis of Cd^{2+} and Pb^{2+}. The detection ranges of Cd^{2+} and Pb^{2+} were 2.0–300 µM and 2.0–300 µM, respectively, and the detection limits were 0.67 µM and 0.17 µM, respectively.
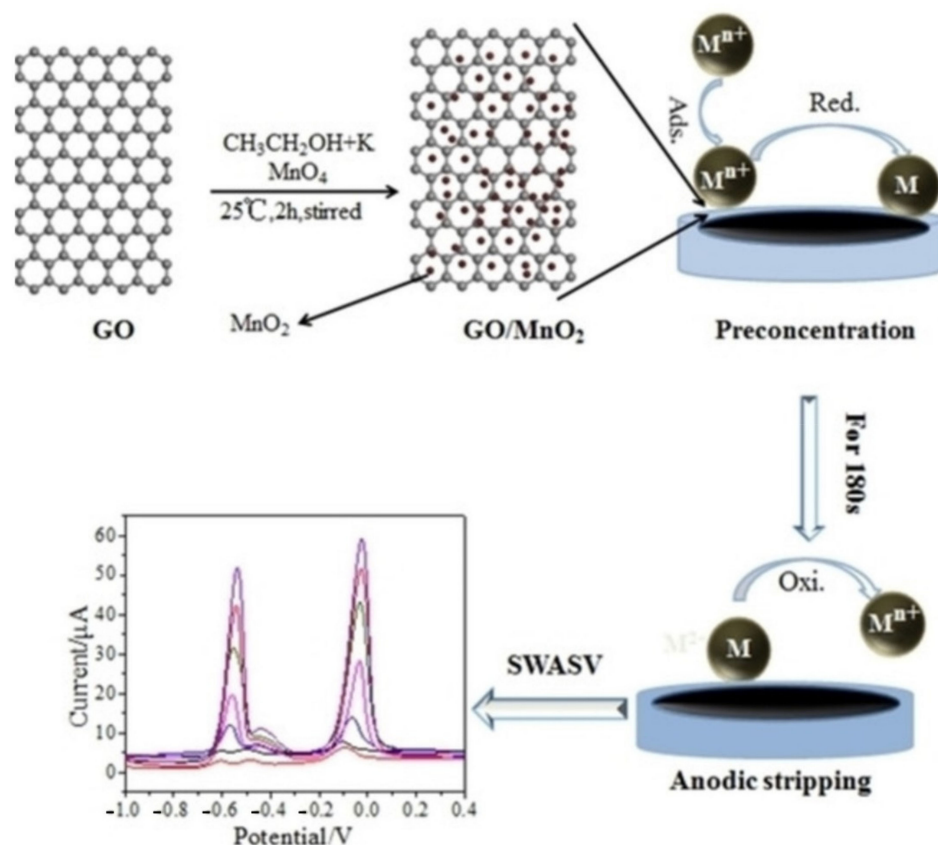

Figure 7. Schematic presentation on the fabrication of GO and MnO$_2$-based electrochemical Cu^{2+} and Pb^{2+} sensors. Reprinted with permission from Ref. [188].

4.1.3. Detection of Antibiotics and Pesticides

Antibiotics and pesticide residues of animal and plant products in food safety have attracted more and more attention [190]. Long-term consumption of foods containing antibiotic residues may cause complications such as antibiotic resistance and allergic reactions. Therefore, it is very important to develop simple, sensitive and reliable methods to determine antibiotics and pesticide residues in food. Jiao et al. [191] prepared a novel composite membrane composed of carbon black and GO@Fe$_3$O$_4$. Based on this membrane, an electrochemical aptamer sensor with high sensitivity and selectivity was developed for the detection of a poisonous maidservant, and the detection limit reached 0.033 ng/mL. Zhou et al. [192] constructed an electrochemical sensor for the detection of pesticide residues using carboxylated graphene as the substrate and compounding SnO$_2$ nanoparticles to form composites. Due to the synergistic effect between SnO$_2$ nanoparticles and graphene, the composite had excellent electrical conductivity, electrocatalytic activity, and biocompatibility. The sensor could be used for sensitive detection of methyl parathion and carbofuran. The detection limits were 0.05 pM and 0.5 pM, respectively,

and the linear detection ranges were 0.1 pM–0.1 nM, 0.1 nM–10 nM, 1 pM–0.1 nM and 0.1 nM–10 nM, respectively.

In addition to graphene, other graphene-like 2DMs were utilized for the fabrication of electrochemical sensors for the detection of pesticide residues. For example, Kokulnathan et al. [193] used 2D BN and bismuth oxide to prepare electrochemical sensors for the detection of flutamide. Li et al. [194] used graphene embedded with AgNPs to form a multi-layer nanostructure and successfully analyzed and detected malachite green molecules in water. The lowest detection limit was 1×10^{-11} M. Malachite green is an additive mainly used in dyeing and aquaculture and is at risk of causing cancer in humans. Nasir et al. [195] prepared conductive 1T phase transition metal sulfide TMDs nanosheets (MoS_2, $MoSe_2$, WS_2, WSe_2) by tert-butyllithium stripping. Using 1T phase TMDs nanosheets (MoS_2, $MoSe_2$, WS_2, WSe_2) as platforms, indirect electrochemical detection of organophosphorus pesticide fenitrothion was carried out by enzyme inhibition. Compared with the sensors without modification of 1T phase TMDs nanosheets, the sensors modified with MoS_2, $MoSe_2$, WS_2, and WSe_2 nanomaterials showed enhanced electrochemical response. Among them, 1T phase WS_2 was better than all the other three TMD materials. The sensor system can detect fenitrothion pesticides in a wide concentration range of 1~1000 nM, with good linearity (r = 0.987), high sensitivity, and very low detection limit (2.86 nM).

Song et al. [196] prepared a composite of ultra-thin bimetallic alloy nanowires (PdCu NW, PdCo NW, PdNi NW) and monolayer molybdenum disulfide nanosheets (m-MoS_2) with 3D porous structure by one-step synthesis. By using this composite as electrode material, a novel sensor was constructed for electrochemical detection and analysis of omethoate, a typical highly toxic organophosphorus pesticide (Figure 8a). Under the optimal conditions, the linear range of the sensor for omethoate detection was 10^{-13} M~10^{-7} M, and the lowest detection limit reached 0.05 pM. In addition, Song et al. [197] prepared a few layers of N-F co-doped MoS_2 nanosheets by hydrothermal method and then prepared AgNPs-N-F-MoS_2 nanocomposites by a simple in situ growth method, which was used to construct electrochemical sensors for rapid detection of the most commonly used organophosphorus insecticides monocrotophos and chlorpyrifos, as shown in Figure 8b. The linear range for detection of monocrotophos was 10^{-10} ~10^{-6} mg/mL, and the detection limit was 0.05 pg/mL. Similarly, the linear range for chlorpyrifos was 5×10^{-8}~10^{-7} mg/mL and 10^{-7}~10^{-4} mg/mL, and the detection limit was 1 pg/mL. Jiang et al. [198] prepared a composite material of $Ti_3C_2T_x$ by in situ reductions and used it to assemble an electrochemical sensor to detect pesticide residues. Through the synergistic effect between AgNPs and $Ti_3C_2T_x$ nanoparticles, the sensor realized the hypersensitive detection of malathion with a detection limit of 3.27×10^{-15} M and a detection range of 10^{-14}–10^{-8} M.

In addition, Peng et al. [199] prepared layered MoS_2/graphene nanocomposites by solvothermal method and used them as substrates to construct electrochemical sensors for the detection of hydroquinone. It was found that the synergistic effect of nanomaterials makes the nanocomposites have good electrocatalytic performance for the electrochemical reaction of hydroquinone. Under the optimal conditions, the MoS_2/graphene-modified electrode could be used for sensitive detection of hydroquinone in the range of 1–9 nM, with a detection limit of 0.3 nM. In addition, the fabricated electrochemical sensor exhibited good stability, selectivity, and reproducibility. In another case, Wu et al. [200] used hydrofluoric acid as raw material to peel off the original phase of Ti_3AlC_2 to obtain MXene-Ti_3C_2 2DMs with electrical conductivity equivalent to that of multilayer graphene. Because Mxene-Ti_3C_2 has metal conductivity, biocompatibility, and good aqueous phase dispersion, the prepared Mxene-Ti_3C_2 was used as the matrix for immobilization of tyrosinase, and an electrochemical sensor was constructed to realize the ultra-sensitive and rapid detection of phenol. The linear range was 0.05–15.5 μM, the detection limit was 12 nM, and the sensitivity was 414.4 mA mol L^{-1}.
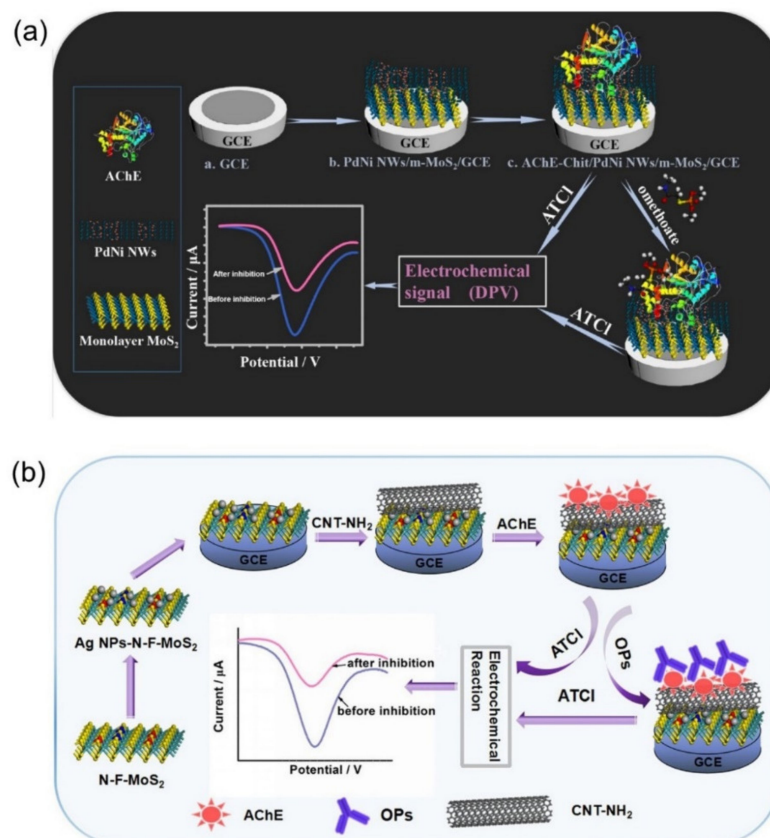
Figure 8. (**a**) Schematic illustration of the fabrication process of the electrochemical biosensor for omethoate assay [196]. (**b**) Schematic illustration of the fabrication process of the electrochemical biosensor for determination of monocrotophos and chlorpyrifos [197].

4.2. 2DM-Based Electrochemical Sensors/Biosensors for Biomolecular Detection

Electrochemical sensors have realized the transformation from ion and gas electrodes to biological electrodes. At the same time, the vigorous development of biotechnology also provided great help to the development of electrochemical biosensors. Because the electrochemical biosensor has the advantages of both electrochemical and biological detection, it received extensive attention and played an important role in the field of sensors [201,202]. The nanomaterials suitable for the construction of electrochemical biosensors should have the following characteristics: (1) good electrical conductivity; (2) the surface area is large enough to provide a wider contact surface for the tested molecules; (3) good biocompatibility; (4) good biological stability and can still work normally after being preserved for a period of time; (5) low cost, simple, and environmentally friendly manufacturing process.

4.2.1. Detection of Glucose, AA, UA, and Other Small Molecules

2DMs have a large specific surface area and can absorb a large number of substances to be measured, which is conducive to the increase in electron transfer rate, electrochemical reaction rate, and detection sensitivity [203]. Therefore, 2DMs have a good application prospect in the detection of small biological molecules. At present, it has been applied to the detection of H_2O_2, glucose, ascorbic acid (AA), uric acid (UA), dopamine (DA), tryptophan, and other small biological molecules [204–206].

For example, Wu et al. [207] used the exfoliated MoS_2 nanosheets to be reduced by electrochemical reduction in NaCl solution to produce reduced MoS_2 ($rMoS_2$). The resulting $rMoS_2$ can detect glucose molecules by immobilization of GOx, and can selectively detect DA in the presence of UA and AA. Song et al. [208] firstly combined the benzoic acid group with reduced graphene oxide via a C-C bond to obtain benzoic acid-functionalized rGO (BFrGO). Then, BFrGO was immersed in a solution containing Co^{2+} and pyromellitic

acid to form BFrGO/Co-MOFs step by step, and then BFrGO/Co-MOFs were decomposed by high-temperature calcination to obtain novel porous cobalt nanospheres/rGO nanocomposites, as shown in Figure 9. A novel electrochemical sensor for glucose detection was constructed based on porous cobalt nanospheres/rGO nanocomposites. Porous cobalt nanospheres/rGO nanocomposites have porous and interfacial layering, good electrical conductivity, and a large specific surface area, so the sensor has good detection performance for glucose, and the detection range was 5–1200 μM, the detection limit was 0.31 μM.
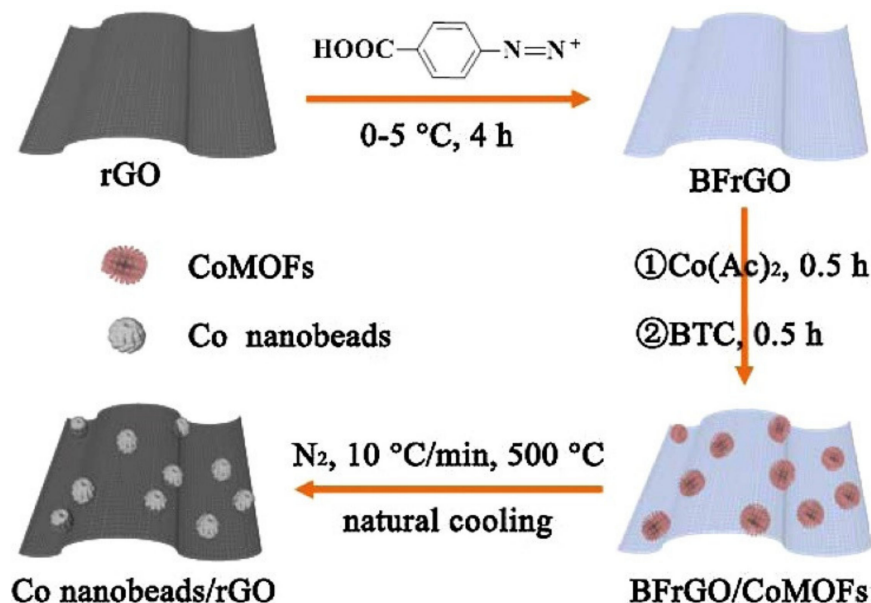

Figure 9. Schematic illustrating preparation process of 3D hierarchical Co nanobeads/rGO nanocomposites. Reprinted with permission from Ref. [208].

Huang et al. [23] modified copper nanoparticles (Cu NPs) onto MoS_2 nanoflakes by chemical reduction. The composite sensor for the detection of glucose showed synergistic electrocatalytic oxidation activity with a sensitivity of 1055 $\mu A\ mM^{-1}\ cm^{-2}$ and a linear range of more than 4 mmol L^{-1}. Parlak et al. [209] constructed the MoS_2/AuNPs interface on the surface of a glassy carbon electrode by electrostatic adsorption, which not only accelerated the surface electrocatalytic reaction but also showed excellent electrochemical performance, such as high current density, electron transfer rate, fast mass transfer rate and so on. The constructed MoS_2/Au NPs/GOx sensor interface has a good linear range of 0.25~13.2 mmol L^{-1} in the detection of glucose, the detection limit was 0.042 μmol L^{-1}, and the sensitivity was 13.80 $\mu A\ \mu\ M^{-1}\ cm^{-2}$. In addition, Kavitha et al. [210] prepared graphene-ZnO nanosheets for glucose detection by glucose sensor, and the sensitivity to glucose was improved by composite materials. Liu et al. [211] developed a sensor for the detection of glucose by using Cu_2O nanocubes-modified graphene nanosheets as electrodes. The sensor has a linear response to glucose in the concentration range of 0.3~3.3 mM, with a detection limit of 3.3 mM, high selectivity, and a short response time. Compared with unloaded Cu_2O nanocubes, graphene-coated Cu_2O nanocubes have higher catalytic activity for glucose oxidation, higher sensitivity, and lower detection limit. Wang et al. [212] prepared an electrode that highly dispersed palladium nanoparticles on graphene for the detection of glucose by electrochemical sensors.

4.2.2. Detection of H_2O_2 and Other Small Molecules Related to Diseases

Reactive oxygen species (ROS), which play an important role in cell metabolism, are markers of progressive neurodegenerative diseases such as Alzheimer's disease, Parkinson's disease, and cancer. H_2O_2 can spread freely through the cell membrane and is a typical representative of ROS in organisms [213,214]. Controlling the content of H_2O_2 at an appropriate level is very important for the intracellular signaling pathway of normal cells,

so it is necessary to monitor the level of H_2O_2 in the biological environment, especially in the cellular environment. Wang et al. [215] synthesized Ti_3C_2 nanosheets and used them to immobilize hemoglobin (Hb) to construct a mediator-free H_2O_2 biosensor with high stability and low detection limit. The experimental results show that Ti_3C_2 nanosheets show excellent biocompatibility to hemoglobin and maintain good biological activity and stability of hemoglobin. The sensor promotes the electron transfer of hemoglobin and shows excellent H_2O_2 detection performance. The detection range was 0.1–260 μM, and the detection limit was 20 nM. Lorencova et al. [24] detected the H_2O_2 of the synthesized Ti_3C_2 nanosheets in the cathodic potential. The experimental results show that Ti_3C_2 is an excellent catalyst for H_2O_2 reduction, and the detection limit of the sensor was as low as 0.7 nM, which is comparable to that of the best reported H_2O_2 sensor (0.3 nM). Tian et al. [216] obtained ultra-thin g-C_3N_4 nanosheets by liquid phase stripping of g-C_3N_4 bulk materials and studied the electrochemical properties of the materials. It was found that g-C_3N_4 nanosheets also had good electrocatalytic activity for H_2O_2 reduction.

In addition, 2DMs have a layered structure and a large specific surface area, which enables this material to be used as a substrate for other nanomaterials, including precious metals, transition metals, carbon materials, and conductive polymers. The combination of this nanomaterial further improves the performance of its electrochemical sensor. Therefore, the modification of precious metal nanoparticles on the surface of 2DMs is an effective method to increase electrochemical signals, of which gold nanoparticles are the most commonly used because AuNPs have excellent electrical properties and biocompatibility [217–219]. For example, Au modified MoS_2 complex can detect AA, DA, and UA at the same time [220]. In addition, the sensor has an electrocatalytic activity for the oxidation of bisphenol A, the linear range was 0.05–100 μM, and the detection limit was 5.0×10^{-9} M [221]. Zhang et al. [222] synthesized AuNPs-rGO through a one-step method. AuNPs can be uniformly loaded on flake graphene, and the size of AuNPs can meet the expected requirements (2–3 nm). The detection limit of AuNPs-rGO modified glassy carbon electrode for H_2O_2 was 0.45 mM, and the detection sensitivity was 283 μA mM^{-1} in the range of 10–130 μM hydrogen peroxide.

Shu et al. [223] constructed an electrochemical H_2O_2 biosensor based on MoS_2 nanosheets–Au nanorods (Au NRs) complex to measure the release of H_2O_2 from living cells (as shown in Figure 10a). Firstly, the MoS_2-Au NRs complex, which combines the advantages of MoS_2 nanosheets and Au NRs, was prepared, and catalase (CAT) was immobilized on the surface of GCE. The unsaturated sulfur atoms at the edge of MoS_2 nanowires can control the aggregation of nanoparticles. The large specific surface area of MoS_2 nanosheets and the good biocompatibility of Au NRs enable the immobilized CAT to retain its natural structure and biological activity. In the real-time monitoring of H_2O_2 released from SP2/0 cells, N-formyl-methionyl-leucyl-phenylalanine (fMLP) was selected as a stimulant for the cell to generate H_2O_2. The $1 \times$ PBS buffer solution without cells (red line in Figure 10a) and $1 \times$ PBS buffer solution with cells and catalase (blue line) show no current change. While after the addition of fMLP, a significantly increased current was observed at the CAT/MoS_2-Au/chitosan/GCE electrode, further suggesting that H_2O_2 was released from cells under the stimulation of fMLP. The results demonstrate that the constructed biosensor is sensitive and reliable for intracellular H_2O_2 detection. The biosensor revealed high sensitivity (187.4 mA M^{-1} cm^{-2}), wide linear range (5.0×10^{-7} M~2.0×10^{-4} M), high selectivity and stability for H_2O_2 detection, and can be used to determine the trace concentration of H_2O_2 released by SP2/0 cells (detection limit of 0.1 μM). Su et al. [224] modified a multifunctional electrochemical sensor with MoS_2-PBNCs nanocomposites (Figure 10b). The electrochemical sensor is used to detect the concentration of hydrogen peroxide and carcinoembryonic antigen, so it can be used in electrochemical catalysis and biomolecule detection.
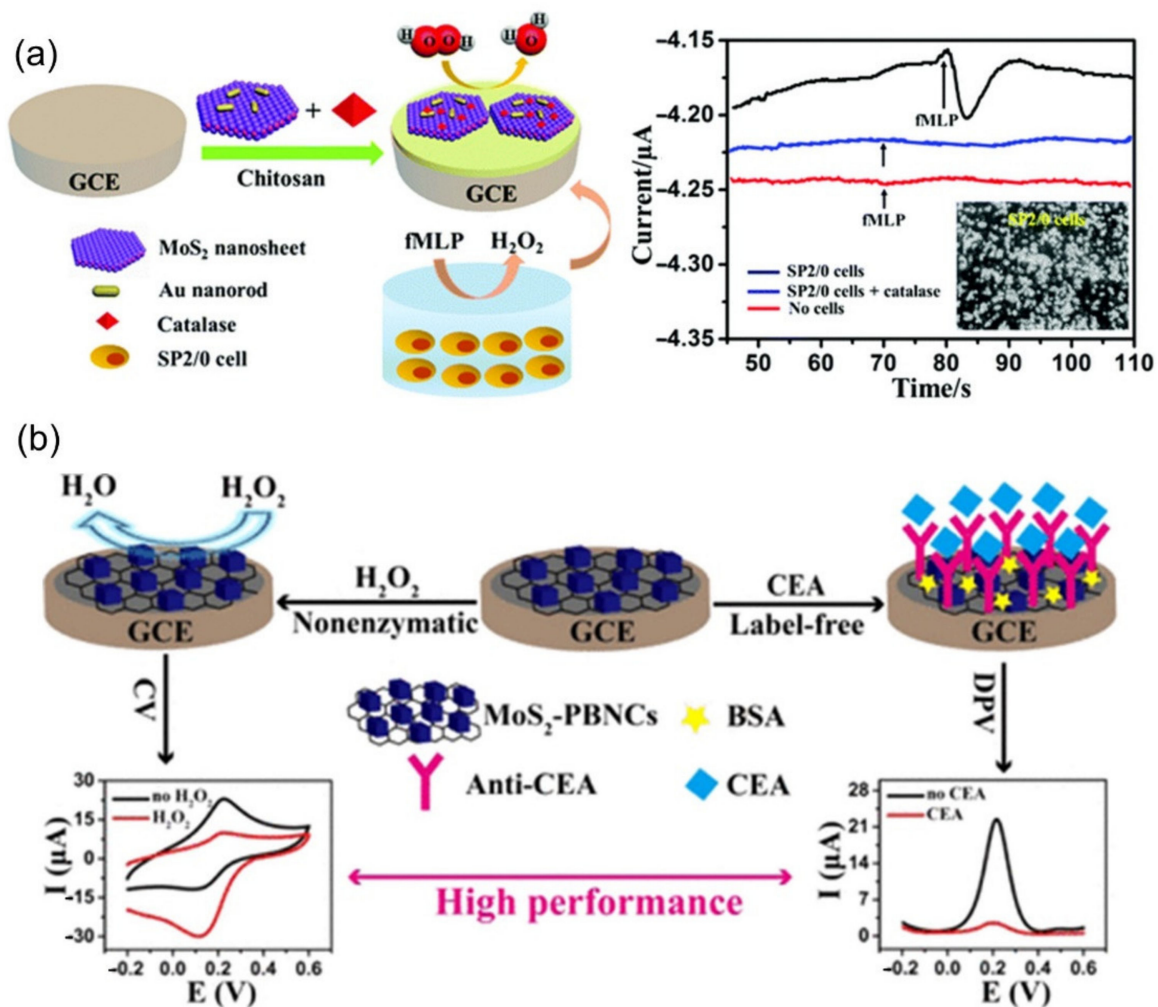
Figure 10. (**a**) Schematic of the catalase/MoS$_2$–Au/chitosan modified GCE used for detecting H$_2$O$_2$ released from cells stimulated with fMLP (left) and Amperometric responses of the CAT/MoS$_2$–Au/chitosan/GCE for the reduction in H$_2$O$_2$ released from about 8.0×10^7 SP$_2$/0 cells in 4 mL 1× PBS (pH 7.4) solution upon addition of 5 µM fMLP (right) [223]. (**b**) Illustration of MoS$_2$-based electrochemical sensors for H$_2$O$_2$ (left) and CEA (right) Detection [224].

In addition to metal nanoparticles, carbon materials, conductive polymers, and transition metals can also be used to modify nanosheets to improve their conductivity and surface area, thus improving electrochemical properties [225–227]. For example, Liu et al. [228] combined MoS$_2$ with rGO hydrothermally to successfully synthesize MoS$_2$-rGO composites, as shown in Figure 11. Then it was used to immobilize Hb, and a mediator-free biosensor was successfully constructed. The electrode showed an excellent electrochemical response to hydrogen peroxide with a wide detection range (0.1~250 µM), a high sensitivity of 346.6 µA mM^{-1} cm^{-2} and a detection limit of 25 nM. Wang et al. [145] successfully loaded TiO$_2$ nanoparticles on Ti$_3$C$_2$ MXene materials to prepare TiO$_2$-Ti$_3$C$_2$ nanocomposites with excellent properties and immobilized Hb on the surface of the composites to build a dielectric-free biosensor. The unique accordion-like structure of the composite accelerates the direct electron transfer rate of Hb, and the sensor showed excellent sensing performance in the detection and analysis of H$_2$O$_2$, with a sensitivity of 447.3 µA mmol L^{-1} cm^{-2}, a linear range of 0.1~380 µM, and a very low detection limit of 14 nM.
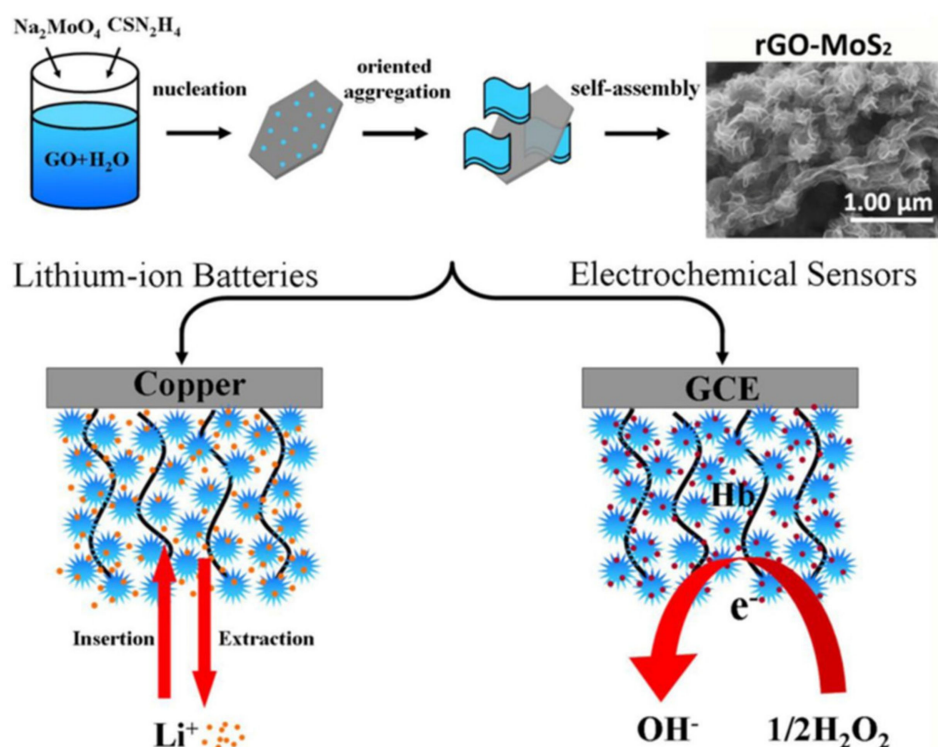
Figure 11. Schematic diagram of the applications of the MoS$_2$-rGO hybrid material in Li-ion battery and electrochemical sensors [228].

4.2.3. Detection of Medical Drugs, DNA, Protein, Antigen, and Others

The detection of other small molecules can be achieved by 2DM-based electrochemical sensors. For instance, Wang et al. [229] fabricated an electrochemical aptamer sensor based on AuNP-modified MoS$_2$ nanosheets and β-cyclodextrin (MoS$_2$-AuNPs-β-CD), which was developed for the hypersensitive detection of ochratoxin A (OTA). Using MoS$_2$ as the dispersion template, MoS$_2$-AuNPs nanocomposites with unique characteristics and functions were prepared by the in situ chemical reduction method. AuNPs promoted electron transfer, improved capture efficiency, and amplified the sensing signal. The constructed sensor realizes the detection of OTA with high sensitivity and selectivity. In another case, Jiang et al. [230] designed and prepared Ti$_3$C$_2$ MXene (ZnON/Ti$_3$C$_2$) heterostructure modified by ZnO quantum dots with high nitrogen doping level through simple heat treatment using glycine as an N precursor. By using it as an efficient electrochemical sensing platform, an electrochemical sensor sensitive and selective to chloramphenicol was constructed, which exhibited a wide linear range (0.1 ng/mL~100 ng/mL), low detection limit (0.019 ng/mL), and high stability. Gu et al. [231] prepared layered composites from graphene and *g*-C$_3$N$_4$ nanosheets and modified them on the surface of GCE. By using the properties of the composites to promote electron transfer and optimize redox current, a series of small biological molecules, including uric acid, norepinephrine, tryptophan, paracetamol, and rutin could be detected successfully.

To make it more clear, Table 1 summarizes the performance of small molecule electrochemical sensors based on different 2DMs.

Table 1. The performances of small molecule electrochemical sensors based on different 2DMs.

Sensor Materials	Analyte	Range of Detection	Detection Limit	Refs.
MoS_2	H_2O_2	5.0–100 nM	2.5 nM	[232]
MoS_2-graphene-horseradish peroxidase	H_2O_2	0.2 μM–1.103 mM	0.049 μM	[233]
MoS_2-PtW	H_2O_2	1–0.2 mM	5 nM	[234]
MoS_2-Cu nanoflower	H_2O_2/glucose	0.04–1.88 μM/1–20 μM	0.021 μM/0.32 μM	[235]
MoS_2-Ni NP	Glucose	0–4 mM	0.31 μM	[102]
MoS_2-Au NP-glucose oxidase	Glucose	10–300 μM	2.8 μM	[236]
MoS_2-PANI-Au NP	DA	1–500 μM	0.1 μM	[237]
MoS_2-Au NP	DA	0.1–200 μM	80 nM	[238]
rGO	UA	0.02–0.49 mM	3.45 μM	[239]
MoS_2-Ag	Tryptophan	0.5–120 μM	0.05 μM	[240]
MoS_2- self-doped polyaniline	Chloramphenicol	0.1–1000 μM	6.5×10^{-8} M	[241]

In addition, electrochemical sensors based on 2DMs and their composites can also be used in other biosensor fields, such as nucleic acid detection, protein detection, and so on. For example, Liu et al. [4] constructed a novel electrochemical immunosensor with a double-antibody sandwich structure based on rGO-Au NPs modified GCE, which was used to determine procalcitonin (PCT), a marker of septicemia. This method was successfully applied to the determination of PCT in blood samples. Yola et al. [242] constructed an electrochemical sensor based on GO-AuNPs to determine the content of tyrosine (Tyr) in milk. The detection limit could reach 0.15 nM. As a biomarker, Tyr is an important part of neurotransmitters, signal transduction systems, and hormones in the human brain [243]. It can prevent aging and senile dementia. It also has electrochemical activity and can be detected directly by electrochemical methods without other indirect processes such as derivatization. Wang et al. [104] proposed a sandwich structure immunosensor, which is a carcinoembryonic antigen (CEA) biosensor based on the MoS_2-Au complex. The MoS_2-Au complex is used to immobilize the first antibody (Ab1) of CEA, and the Ag nanoparticles are used to support the second antibody (Ab2) and GOx of CEA. When glucose exists in the system, the resulting H_2O_2 is catalyzed by the MoS_2-Au complex, and the reduction peak can be detected. The immunosensor had a linear relationship in the range of 1–50 ng mL^{-1}, and its detection limit could reach 0.27 pg mL^{-1}. Huang et al. [244] also reported an electrochemical immunosensor using graphene nanocomposites coated with Ag/AuNPs to modify the bare working electrode for hypersensitive detection of carcinoembryonic antigen.

5. Conclusions and Future Perspectives

Based on the above introduction and discussion, it can be concluded that 2DM-based electrochemical sensors have significant advantages in substance detection, such as convenience and speed, simple operation, low cost, and short time consumption. They have excellent performance in food safety, environmental monitoring, biological science, pharmaceutical industry, and other fields. As a new research field in recent years, the development and application of electrochemical sensors based on 2DMs provide a new research topic for the detection of pesticide residues, heavy metal ion detection, and biological small molecule detection. This review mainly introduces the preparation methods, structures, and properties of 2DMs and their applications in various electrochemical detection. Through the design of functional nanomaterials and the construction of sensing electrodes, the test performance of electrochemical sensors is improved.

However, there are still some problems in the use of 2DM-modified electrodes for electrochemical sensor applications. (1) The preparation process of some nanomaterials is cumbersome, with poor repeatability and low service life, which seriously reduces the reliability of the test results. (2) Most nano-sensing materials and electrodes are bound by physical interaction, and the weak binding strength affects the stability of the sensor test. In order to solve the above problems, the following solutions can be taken. First, the design and synthesis of new nanomaterials with excellent electrochemical performance and stable structure are needed, which can significantly improve the reproducibility and reliability

of sensing tests. Second, novel fabrication techniques for modifying electrodes should be explored and developed. By continuously improving the bonding mechanism between nanomaterials and modified electrodes, the bonding strength of nanomaterials on the electrode surface can be improved to enhance the stability and easy detachment of nanomaterial modifications on the electrode, thereby improving the stability of electrochemical detection.

Author Contributions: Conceptualization, T.L., D.S. and G.W.; reference analysis, T.L., D.S., S.G., B.W., P.X. and W.S.; resources, all authors; writing—original draft preparation, T.L. and D.S.; writing—review and editing, T.L., H.K., G.Y. and G.W.; supervision, G.W.; project administration, T.L. and G.W.; funding acquisition, G.W. All authors have read and agreed to the published version of the manuscript.

Institutional Review Board Statement: Not applicable.

Informed Consent Statement: Not applicable.

Data Availability Statement: Not applicable.

Conflicts of Interest: The authors declare no conflict of interest.

References

1. Rassaei, L.; Amiri, M.; Cirtiu, C.M.; Sillanpaa, M.; Marken, F.; Sillanpaa, M. Nanoparticles in electrochemical sensors for environmental monitoring. *Trends Anal. Chem.* **2011**, *30*, 1704–1715. [CrossRef]
2. Viswanathan, S.; Radecka, H.; Radecki, J. Electrochemical biosensors for food analysis. *Monatsh. Chem.* **2009**, *140*, 891–899. [CrossRef]
3. Fu, J.Y.; An, X.S.; Yao, Y.; Guo, Y.M.; Sun, X. Electrochemical aptasensor based on one step co-electrodeposition of aptamer and GO-CuNPs nanocomposite for organophosphorus pesticide detection. *Sens. Actuators B Chem.* **2019**, *287*, 503–509. [CrossRef]
4. Liu, F.; Xiang, G.M.; Yuan, R.; Chen, X.M.; Luo, F.K.; Jiang, D.N.; Huang, S.G.; Li, Y.; Pu, X.Y. Procalcitonin sensitive detection based on graphene-gold nanocomposite film sensor platform and single-walled carbon nanohorns/hollow Pt chains complex as signal tags. *Biosens. Bioelectron.* **2014**, *60*, 210–217. [CrossRef] [PubMed]
5. Zhou, Y.L.; Yin, H.S.; Li, J.; Li, B.C.; Li, X.; Ai, S.Y.; Zhang, X.S. Electrochemical biosensor for microRNA detection based on poly (U) polymerase mediated isothermal signal amplification. *Biosens. Bioelectron.* **2016**, *79*, 79–85. [CrossRef]
6. Nikolaus, N.; Strehlitz, B. Amperometric lactate biosensors and their application in (sports) medicine, for life quality and wellbeing. *Microchim. Acta* **2008**, *160*, 15–55. [CrossRef]
7. Li, T.; Sun, M.C.; Wu, S.H. State-of-the-Art Review of Electrospun Gelatin-Based Nanofiber Dressings for Wound Healing Applications. *Nanomaterials* **2022**, *12*, 784. [CrossRef]
8. Liu, J.; Li, T.; Zhang, H.; Zhao, W.; Qu, L.; Chen, S.; Wu, S. Electrospun strong, bioactive, and bioabsorbable silk fibroin/poly (L-lactic-acid) nanoyarns for constructing advanced nanotextile tissue scaffolds. *Mater. Today Bio* **2022**, *14*, 100243. [CrossRef]
9. He, J.Y.; Xu, P.L.; Zhou, R.F.; Li, H.; Zu, H.L.; Zhang, J.; Qin, Y.B.; Liu, X.H.; Wang, F.Y. Combustion Synthesized Electrospun InZnO Nanowires for Ultraviolet Photodetectors. *Adv. Electron. Mater.* **2021**, *8*, 2100997. [CrossRef]
10. Sheng, X.L.; Li, T.; Sun, M.; Liu, G.J.; Zhang, Q.; Ling, Z.B.; Gao, S.W.; Diao, F.Y.; Zhang, J.Z.; Rosei, F.; et al. Flexible electrospun iron compounds/carbon fibers: Phase transformation and electrochemical properties. *Electrochim. Acta* **2022**, *407*, 139892. [CrossRef]
11. Valiev, R. Materials science—Nanomaterial advantage. *Nature* **2002**, *419*, 887–889. [CrossRef] [PubMed]
12. Yu, H.; Jian, X.; Jin, J.; Wang, F.; Wang, Y.; Qi, G.C. Preparation of hybrid cobalt-iron hexacyanoferrate nanoparticles modified multi-walled carbon nanotubes composite electrode and its application. *J. Electroanal. Chem.* **2013**, *700*, 47–53. [CrossRef]
13. Li, H.; Xu, P.L.; Liu, D.; He, J.Y.; Zu, H.L.; Song, J.J.; Zhang, J.; Tian, F.H.; Yun, M.J.; Wang, F.Y. Low-voltage and fast-response SnO$_2$ nanotubes/perovskite heterostructure photodetector. *Nanotechnology* **2021**, *32*, 375202. [CrossRef] [PubMed]
14. Zeng, Z.Y.; Yin, Z.Y.; Huang, X.; Li, H.; He, Q.Y.; Lu, G.; Boey, F.; Zhang, H. Single-Layer Semiconducting Nanosheets: High-Yield Preparation and Device Fabrication. *Angew. Chem. Int. Ed.* **2011**, *50*, 11093–11097. [CrossRef] [PubMed]
15. Xu, D.M.; Chao, D.L.; Wang, H.W.; Gong, Y.S.; Wang, R.; He, B.B.; Hu, X.L.; Fan, H.J. Flexible Quasi-Solid-State Sodium-Ion Capacitors Developed Using 2D Metal-Organic-Framework Array as Reactor. *Adv. Energy Mater.* **2018**, *8*, 1702769. [CrossRef]
16. Kotekar-Patil, D.; Deng, J.; Wong, S.L.; Lau, C.S.; Goh, K.E.J. Single layer MoS$_2$ nanoribbon field effect transistor. *Appl. Phys. Lett.* **2019**, *114*, 013508. [CrossRef]
17. Zhang, X.M.; Zhao, Y.X.; Wu, Y.T.; Mao, Z.X. Two-Dimensional Hexagonal NiCo$_2$O$_4$ Nanoplates@PEDOT/RGO Nanocomposite: A Design and Construction High Selective H$_2$O$_2$ Sensing Interface. *J. Electrochem. Soc.* **2020**, *167*, 067519. [CrossRef]

18. Kumar, J.V.; Mutharani, B.; Chen, S.M.; Rajakumaran, R.; Nagarajan, E.R. Exploring the electrocatalytic application of two-dimensional samarium molybdate (gamma-Sm-3(MoO$_4$)(3)) nanoplatelets for the selective sensing of the organophosphate insecticide oxyparathion. *New J. Chem.* **2020**, *44*, 4285–4294. [CrossRef]

19. Jiang, F.; Zhao, W.S.; Zhang, J. Mini-review: Recent progress in the development of MoSe$_2$ based chemical sensors and biosensors. *Microelectron. Eng.* **2020**, *225*, 111279. [CrossRef]

20. Guo, Y.L.; Wu, B.; Liu, H.T.; Ma, Y.Q.; Yang, Y.; Zheng, J.; Yu, G.; Liu, Y.Q. Electrical Assembly and Reduction of Graphene Oxide in a Single Solution Step for Use in Flexible Sensors. *Adv. Mater.* **2011**, *23*, 4626–4630. [CrossRef]

21. He, Q.Y.; Zeng, Z.Y.; Yin, Z.Y.; Li, H.; Wu, S.X.; Huang, X.; Zhang, H. Fabrication of Flexible MoS$_2$ Thin-Film Transistor Arrays for Practical Gas-Sensing Applications. *Small* **2012**, *8*, 2994–2999. [CrossRef] [PubMed]

22. Lee, M.H.; Thomas, J.L.; Su, Z.L.; Yeh, W.K.; Monzel, A.S.; Bolognin, S.; Schwamborn, J.C.; Yang, C.H.; Lin, H.Y. Transition metal dichalcogenides to optimize the performance of peptide-imprinted conductive polymers as electrochemical sensors. *Microchim. Acta* **2021**, *188*, 203. [CrossRef]

23. Huang, J.W.; Dong, Z.P.; Li, Y.R.; Li, J.; Tang, W.J.; Yang, H.D.; Wang, J.; Bao, Y.; Jin, J.; Li, R. MoS$_2$ nanosheet functionalized with Cu nanoparticles and its application for glucose detection. *Mater. Res. Bull.* **2013**, *48*, 4544–4547. [CrossRef]

24. Lorencova, L.; Bertok, T.; Dosekova, E.; Holazova, A.; Paprckova, D.; Vikartovska, A.; Sasinkova, V.; Filip, J.; Kasak, P.; Jerigova, M.; et al. Electrochemical performance of Ti$_3$C$_2$Tx MXene in aqueous media: Towards ultrasensitive H$_2$O$_2$ sensing. *Electrochim. Acta* **2017**, *235*, 471–479. [CrossRef] [PubMed]

25. Lorencova, L.; Bertok, T.; Filip, J.; Jerigova, M.; Velic, D.; Kasak, P.; Mahmoud, K.A.; Tkac, J. Highly stable Ti$_3$C$_2$Tx (MXene)/Pt nanoparticles-modified glassy carbon electrode for H$_2$O$_2$ and small molecules sensing applications. *Sens. Actuators B Chem.* **2018**, *263*, 360–368. [CrossRef]

26. Gan, X.R.; Zhao, H.M.; Quan, X. Two-dimensional MoS$_2$: A promising building block for biosensors. *Biosens. Bioelectron.* **2017**, *89*, 56–71. [CrossRef]

27. Novoselov, K.S.; Jiang, D.; Schedin, F.; Booth, T.J.; Khotkevich, V.V.; Morozov, S.V.; Geim, A.K. Two-dimensional atomic crystals. *Proc. Natl. Acad. Sci. USA* **2005**, *102*, 10451–10453. [CrossRef]

28. Lee, J.; Dak, P.; Lee, Y.; Park, H.; Choi, W.; Alam, M.A.; Kim, S. Two-dimensional Layered MoS$_2$ Biosensors Enable Highly Sensitive Detection of Biomolecules. *Sci. Rep.* **2014**, *4*, 7352. [CrossRef]

29. Sarkar, D.; Liu, W.; Xie, X.J.; Anselmo, A.C.; Mitragotri, S.; Banerjee, K. MoS$_2$ Field-Effect Transistor for Next-Generation Label-Free Biosensors. *Acs Nano* **2014**, *8*, 3992–4003. [CrossRef]

30. Li, H.; Liu, B.; Cai, D.P.; Wang, Y.R.; Liu, Y.; Mei, L.; Wang, L.L.; Wang, D.D.; Li, Q.H.; Wang, T.H. High-temperature humidity sensors based on WO$_3$-SnO$_2$ composite hollow nanospheres. *J. Mater. Chem. A* **2014**, *2*, 6854–6862. [CrossRef]

31. Huang, Y.; Sutter, E.; Shi, N.N.; Zheng, J.B.; Yang, T.Z.; Englund, D.; Gao, H.J.; Sutter, P. Reliable Exfoliation of Large-Area High-Quality Flakes of Graphene and Other Two-Dimensional Materials. *Acs Nano* **2015**, *9*, 10612–10620. [CrossRef] [PubMed]

32. Yu, X.Y.; Hu, H.; Wang, Y.W.; Chen, H.Y.; Lou, X.W. Ultrathin MoS$_2$ Nanosheets Supported on N-doped Carbon Nanoboxes with Enhanced Lithium Storage and Electrocatalytic Properties. *Angew. Chem. Int. Ed.* **2015**, *54*, 7395–7398. [CrossRef] [PubMed]

33. Huang, X.; Zeng, Z.Y.; Zhang, H. Metal dichalcogenide nanosheets: Preparation, properties and applications. *Chem. Soc. Rev.* **2013**, *42*, 1934–1946. [CrossRef] [PubMed]

34. Zhou, K.G.; Mao, N.N.; Wang, H.X.; Peng, Y.; Zhang, H.L. A Mixed-Solvent Strategy for Efficient Exfoliation of Inorganic Graphene Analogues. *Angew. Chem. Int. Ed.* **2011**, *50*, 10839–10842. [CrossRef]

35. Shi, Y.M.; Li, H.N.; Li, L.J. Recent advances in controlled synthesis of two-dimensional transition metal dichalcogenides via vapour deposition techniques. *Chem. Soc. Rev.* **2015**, *44*, 2744–2756. [CrossRef]

36. Singh, M.; Ghosh, R.; Chen, Y.S.; Yen, Z.L.; Hofmann, M.; Chen, Y.F.; Hsieh, Y.P. Chemical vapor deposition merges MoS$_2$ grains into high-quality and centimeter-scale films on Si/SiO$_2$. *RSC Adv.* **2022**, *12*, 5990–5996. [CrossRef]

37. Xu, Y.H.; Zhu, Y.J.; Han, F.D.; Luo, C.; Wang, C.S. 3D Si/C Fiber Paper Electrodes Fabricated Using a Combined Electrospray/Electrospinning Technique for Li-Ion Batteries. *Adv. Energy Mater.* **2015**, *5*, 1400753. [CrossRef]

38. Liu, H.F.; Wong, S.L.; Chi, D.Z. CVD Growth of MoS$_2$-based Two-dimensional Materials. *Chem. Vap. Depos.* **2015**, *21*, 241–259. [CrossRef]

39. Wang, L.F.; Li, Y.; Zhao, L.; Qi, Z.J.; Gou, J.Y.; Zhang, S.; Zhang, J.Z. Recent advances in ultrathin two-dimensional materials and biomedical applications for reactive oxygen species generation and scavenging. *Nanoscale* **2020**, *12*, 19516–19535. [CrossRef]

40. Zhao, P.; Jian, M.P.; Zhang, Q.; Xu, R.M.; Liu, R.P.; Zhang, X.W.; Liu, H.J. A new paradigm of ultrathin 2D nanomaterial adsorbents in aqueous media: Graphene and GO, MoS$_2$, MXenes, and 2D MOFs. *J. Mater. Chem. A* **2019**, *7*, 16598–16621. [CrossRef]

41. Tan, C.L.; Cao, X.H.; Wu, X.J.; He, Q.Y.; Yang, J.; Zhang, X.; Chen, J.Z.; Zhao, W.; Han, S.K.; Nam, G.H.; et al. Recent Advances in Ultrathin Two-Dimensional Nanomaterials. *Chem. Rev.* **2017**, *117*, 6225–6331. [CrossRef] [PubMed]

42. Xie, H.G.; Li, Z.; Cheng, L.; Haidry, A.A.; Tao, J.Q.; Xu, Y.; Xu, K.; Ou, J.Z. Recent advances in the fabrication of 2D metal oxides. *Iscience* **2022**, *25*, 103598. [CrossRef]

43. Tan, C.L.; Zhang, H. Wet-chemical synthesis and applications of non-layer structured two-dimensional nanomaterials. *Nat. Commun.* **2015**, *6*, 7873. [CrossRef] [PubMed]

44. Xie, J.F.; Zhang, H.; Li, S.; Wang, R.X.; Sun, X.; Zhou, M.; Zhou, J.F.; Lou, X.W.; Xie, Y. Defect-Rich MoS$_2$ Ultrathin Nanosheets with Additional Active Edge Sites for Enhanced Electrocatalytic Hydrogen Evolution. *Adv. Mater.* **2013**, *25*, 5807–5813. [CrossRef] [PubMed]

45. Dong, Y.; Yang, J.T.; Liu, Y.J.; Wang, Y.; Dong, Z.; Cui, M.L.; Li, M.X.; Yuan, X.L.; Zhang, X.; Dai, X.P. 2D Fe-doped NiO nanosheets with grain boundary defects for the advanced oxygen evolution reaction. *Dalton Trans.* **2020**, *49*, 6355–6362. [CrossRef] [PubMed]

46. Won, J.K.; Hwang, C.; Ahn, K.; Choi, S.Y.; Lee, Y.; Kim, J.; Lee, Y.; Park, S.K.; Chung, I.; Kim, C.; et al. Controlled synthesis of SnS$_x$Se$_{2-x}$ nanoplate alloys via synergetic control of reactant activity and surface defect passivation control with surfactant and co-surfactant mixture. *J. Solid State Chem.* **2019**, *278*, 120887. [CrossRef]

47. Meng, Z.; Stolz, R.M.; Mendecki, L.; Mirica, K.A. Electrically-Transduced Chemical Sensors Based on Two Dimensional Nanomaterials. *Chem. Rev.* **2019**, *119*, 478–598. [CrossRef]

48. Zeng, M.Q.; Xiao, Y.; Liu, J.X.; Yang, K.; Fu, L. Exploring Two-Dimensional Materials toward the Next-Generation Circuits: From Monomer Design to Assembly Control. *Chem. Rev.* **2018**, *118*, 6236–6296. [CrossRef]

49. Vlassiouk, I.V.; Stehle, Y.; Pudasaini, P.R.; Unocic, R.R.; Rack, P.D.; Baddorf, A.P.; Ivanov, I.N.; Lavrik, N.V.; List, F.; Gupta, N.; et al. Evolutionary selection growth of two-dimensional materials on polycrystalline substrates. *Nat. Mater.* **2018**, *17*, 318–322. [CrossRef]

50. Geim, A.K.; Grigorieva, I.V. Van der Waals heterostructures. *Nature* **2013**, *499*, 419–425. [CrossRef]

51. Yang, G.Z.; Kong, H.; Chen, Y.; Liu, B.; Zhu, D.Z.; Guo, L.; Wei, G. Recent advances in the hybridization of cellulose and carbon nanomaterials: Interactions, structural design, functional tailoring, and applications. *Carbohydr. Polym.* **2022**, *279*, 118947. [CrossRef] [PubMed]

52. Hu, M.C.; Yao, Z.H.; Wang, X.Q. Graphene-Based Nanomaterials for Catalysis. *Ind. Eng. Chem. Res.* **2017**, *56*, 3477–3502. [CrossRef]

53. Bolotin, K.I.; Sikes, K.J.; Jiang, Z.; Klima, M.; Fudenberg, G.; Hone, J.; Kim, P.; Stormer, H.L. Ultrahigh electron mobility in suspended graphene. *Solid State Commun.* **2008**, *146*, 351–355. [CrossRef]

54. Wang, Y.L.; Chen, Y.A.; Lacey, S.D.; Xu, L.S.; Xie, H.; Li, T.; Danner, V.A.; Hu, L.B. Reduced graphene oxide film with record-high conductivity and mobility. *Mater. Today* **2018**, *21*, 186–192. [CrossRef]

55. Gruneis, A.; Attaccalite, C.; Wirtz, L.; Shiozawa, H.; Saito, R.; Pichler, T.; Rubio, A. Tight-binding description of the quasiparticle dispersion of graphite and few-layer graphene. *Phys. Rev. B* **2008**, *78*, 205425. [CrossRef]

56. Zhang, T.; Liu, J.L.; Wang, C.; Leng, X.Y.; Xiao, Y.; Fu, L. Synthesis of graphene and related two-dimensional materials for bioelectronics devices. *Biosens. Bioelectron.* **2017**, *89*, 28–42. [CrossRef]

57. Sohn, I.Y.; Kim, D.J.; Jung, J.H.; Yoon, O.J.; Thanh, T.N.; Quang, T.T.; Lee, N.E. pH sensing characteristics and biosensing application of solution-gated reduced graphene oxide field-effect transistors. *Biosens. Bioelectron.* **2013**, *45*, 70–76. [CrossRef]

58. Xie, Z.J.; Duo, Y.H.; Lin, Z.T.; Fan, T.J.; Xing, C.Y.; Yu, L.; Wang, R.H.; Qiu, M.; Zhang, Y.P.; Zhao, Y.H.; et al. The Rise of 2D Photothermal Materials beyond Graphene for Clean Water Production. *Adv. Sci.* **2020**, *7*, 1902236. [CrossRef]

59. Wu, J.S.; Pisula, W.; Mullen, K. Graphenes as potential material for electronics. *Chem. Rev.* **2007**, *107*, 718–747. [CrossRef]

60. Agudosi, E.S.; Abdullah, E.C.; Numan, A.; Mubarak, N.M.; Khalid, M.; Omar, N. A Review of the Graphene Synthesis Routes and its Applications in Electrochemical Energy Storage. *Crit. Rev. Solid State Mater. Sci.* **2020**, *45*, 339–377. [CrossRef]

61. Liu, Y.X.; Dong, X.C.; Chen, P. Biological and chemical sensors based on graphene materials. *Chem. Soc. Rev.* **2012**, *41*, 2283–2307. [CrossRef] [PubMed]

62. Hossain, M.F.; Park, J.Y. An Enzymatic Hybrid Electrode Platform Based on Chemically Modified Reduced Graphene Oxide Decorated with Palladium and Platinum Alloy Nanoparticles for Biosensing Applications. *J. Electrochem. Soc.* **2015**, *162*, B185–B192. [CrossRef]

63. Yusof, N.M.; Ibrahim, S.; Rozali, S. Advances on graphene-based gas sensors for acetone detection based on its physical and chemical attributes. *J. Mater. Res.* **2022**, *37*, 405–423. [CrossRef]

64. Chen, Y.; Yang, G.Z.; Liu, B.; Kong, H.; Xiong, Z.; Guo, L.; Wei, G. Biomineralization of ZrO$_2$ nanoparticles on graphene oxide-supported peptide/cellulose binary nanofibrous membranes for high-performance removal of fluoride ions. *Chem. Eng. J.* **2022**, *430*, 132721. [CrossRef]

65. Yu, X.W.; Cheng, H.H.; Zhang, M.; Zhao, Y.; Qu, L.T.; Shi, G.Q. Graphene-based smart materials. *Nat. Rev. Mater.* **2017**, *2*, 17046. [CrossRef]

66. Jang, H.; Park, Y.J.; Chen, X.; Das, T.; Kim, M.S.; Ahn, J.H. Graphene-Based Flexible and Stretchable Electronics. *Adv. Mater.* **2016**, *28*, 4184–4202. [CrossRef]

67. Wei, X.L.; Chen, Y.P.; Liu, W.L.; Zhong, J.X. Enhanced gas sensor based on nitrogen-vacancy graphene nanoribbons. *Phys. Lett. A* **2012**, *376*, 559–562. [CrossRef]

68. Hussain, T.; Panigrahi, P.; Ahuja, R. Enriching physisorption of H$_2$S and NH$_3$ gases on a graphane sheet by doping with Li adatoms. *Phys. Chem. Chem. Phys.* **2014**, *16*, 8100–8105. [CrossRef]

69. Niu, F.; Liu, J.M.; Tao, L.M.; Wang, W.; Song, W.G. Nitrogen and silica co-doped graphene nanosheets for NO$_2$ gas sensing. *J. Mater. Chem. A* **2013**, *1*, 6130–6133. [CrossRef]

70. Chu, B.H.; Lo, C.F.; Nicolosi, J.; Chang, C.Y.; Chen, V.; Strupinski, W.; Pearton, S.J.; Ren, F. Hydrogen detection using platinum coated graphene grown on SiC. *Sens. Actuators B Chem.* **2011**, *157*, 500–503. [CrossRef]

71. Yi, J.; Lee, J.M.; Park, W.I. Vertically aligned ZnO nanorods and graphene hybrid architectures for high-sensitive flexible gas sensors. *Sens. Actuators B Chem.* **2011**, *155*, 264–269. [CrossRef]

72. Alqarni, S.A.; Hussein, M.A.; Ganash, A.A.; Khan, A. Composite Material-Based Conducting Polymers for Electrochemical Sensor Applications: A Mini Review. *Bionanoscience* **2020**, *10*, 351–364. [CrossRef]

73. Lei, W.; Si, W.M.; Xu, Y.J.; Gu, Z.Y.; Hao, Q.L. Conducting polymer composites with graphene for use in chemical sensors and biosensors. *Microchim. Acta* **2014**, *181*, 707–722. [CrossRef]

74. Liu, Y.; Yu, D.S.; Zeng, C.; Miao, Z.C.; Dai, L.M. Biocompatible Graphene Oxide-Based Glucose Biosensors. *Langmuir* **2010**, *26*, 6158–6160. [CrossRef]

75. Tyagi, P.; Sharma, A.; Tomar, M.; Gupta, V. A comparative study of RGO-SnO_2 and MWCNT-SnO_2 nanocomposites based SO_2 gas sensors. *Sens. Actuators B Chem.* **2017**, *248*, 980–986. [CrossRef]

76. Yu, X.J.; Cheng, C.D.; Feng, S.P.; Jia, X.H.; Song, H.J. Porous alpha-Fe_2O_3 nanorods@graphite nanocomposites with improved high temperature gas sensitive properties. *J. Alloys Compd.* **2019**, *784*, 1261–1269. [CrossRef]

77. Kong, H.; Chen, Y.; Yang, G.Z.; Liu, B.; Guo, L.; Wang, Y.; Zhou, X.; Wei, G. Two-dimensional material-based functional aerogels for treating hazards in the environment: Synthesis, functional tailoring, applications, and sustainability analysis. *Nanoscale Horiz.* **2022**, *7*, 112–140. [CrossRef]

78. Helal, M.A.; El-Sayed, H.M.; Maarouf, A.A.; Fadlallah, M.M. Metal dichalcogenide nanomeshes: Structural, electronic and magnetic properties. *Phys. Chem. Chem. Phys.* **2021**, *23*, 21183–21195. [CrossRef]

79. Barua, S.; Dutta, H.S.; Gogoi, S.; Devi, R.; Khan, R. Nanostructured MoS_2-Based Advanced Biosensors: A Review. *ACS Appl. Nano Mater.* **2018**, *1*, 2–25. [CrossRef]

80. Wang, J.L.; Wei, Y.; Li, H.; Huang, X.; Zhang, H. Crystal phase control in two-dimensional materials. *Sci. China Chem.* **2018**, *61*, 1227–1242. [CrossRef]

81. Yoshida, M.; Ye, J.T.; Zhang, Y.J.; Imai, Y.; Kimura, S.; Fujiwara, A.; Nishizaki, T.; Kobayashi, N.; Nakano, M.; Iwasa, Y. Extended Polymorphism of Two-Dimensional Material. *Nano Lett.* **2017**, *17*, 5567–5571. [CrossRef] [PubMed]

82. Qian, Z.Y.; Jiao, L.Y.; Xie, L.M. Phase Engineering of Two-Dimensional Transition Metal Dichalcogenides. *Chin. J. Chem.* **2020**, *38*, 753–760. [CrossRef]

83. Voiry, D.; Mohite, A.; Chhowalla, M. Phase engineering of transition metal dichalcogenides. *Chem. Soc. Rev.* **2015**, *44*, 2702–2712. [CrossRef] [PubMed]

84. Li, H.; Lu, G.; Yin, Z.Y.; He, Q.Y.; Li, H.; Zhang, Q.; Zhang, H. Optical Identification of Single- and Few-Layer MoS_2 Sheets. *Small* **2012**, *8*, 682–686. [CrossRef] [PubMed]

85. Wu, M.; Xiao, Y.H.; Zeng, Y.; Zhou, Y.L.; Zeng, X.B.; Zhang, L.N.; Liao, W.G. Synthesis of two-dimensional transition metal dichalcogenides for electronics and optoelectronics. *Infomat* **2021**, *3*, 362–396. [CrossRef]

86. Mukundan, A.; Feng, S.W.; Weng, Y.H.; Tsao, Y.M.; Artemkina, S.B.; Fedorov, V.E.; Lin, Y.-S.; Huang, Y.C.; Wang, H.C. Optical and Material Characteristics of MoS_2/Cu_2O Sensor for Detection of Lung Cancer Cell Types in Hydroplegia. *Int. J. Mol. Sci.* **2022**, *23*, 4745. [CrossRef]

87. Li, H.; Yin, Z.Y.; He, Q.Y.; Li, H.; Huang, X.; Lu, G.; Fam, D.W.H.; Tok, A.I.Y.; Zhang, Q.; Zhang, H. Fabrication of Single- and Multilayer MoS_2 Film-Based Field-Effect Transistors for Sensing NO at Room Temperature. *Small* **2012**, *8*, 63–67. [CrossRef]

88. Eda, G.; Fujita, T.; Yamaguchi, H.; Voiry, D.; Chen, M.W.; Chhowalla, M. Coherent Atomic and Electronic Heterostructures of Single-Layer MoS_2. *Acs Nano* **2012**, *6*, 7311–7317. [CrossRef]

89. Acerce, M.; Voiry, D.; Chhowalla, M. Metallic 1T phase MoS_2 nanosheets as supercapacitor electrode materials. *Nat. Nanotechnol.* **2015**, *10*, 313–318. [CrossRef]

90. Yang, Y.; Liu, T.; Cheng, L.; Song, G.S.; Liu, Z.; Chen, M.W. MoS_2-Based Nanoprobes for Detection of Silver Ions in Aqueous Solutions and Bacteria. *ACS Appl. Mater. Interfaces* **2015**, *7*, 7526–7533. [CrossRef]

91. Mao, K.; Wu, Z.T.; Chen, Y.R.; Zhou, X.D.; Shen, A.G.; Hu, J.M. A novel biosensor based on single-layer MoS_2 nanosheets for detection of Ag^+. *Talanta* **2015**, *132*, 658–663. [CrossRef] [PubMed]

92. Ganatra, R.; Zhang, Q. Few-Layer MoS_2: A Promising Layered Semiconductor. *Acs Nano* **2014**, *8*, 4074–4099. [CrossRef] [PubMed]

93. Kalantar-zadeh, K.; Ou, J.Z. Biosensors Based on Two-Dimensional MoS_2. *ACS Sensors* **2016**, *1*, 5–16. [CrossRef]

94. Hu, Z.H.; Wu, Z.T.; Han, C.; He, J.; Ni, Z.H.; Chen, W. Two-dimensional transition metal dichalcogenides: Interface and defect engineering. *Chem. Soc. Rev.* **2018**, *47*, 3100–3128. [CrossRef]

95. Huang, H.X.; Zha, J.J.; Li, S.S.; Tan, C.L. Two-dimensional alloyed transition metal dichalcogenide nanosheets: Synthesis and applications. *Chin. Chem. Lett.* **2022**, *33*, 163–176. [CrossRef]

96. Lin, H.H.; Wang, C.X.; Wu, J.P.; Xu, Z.Z.; Huang, Y.J.; Zhang, C. Colloidal synthesis of MoS_2 quantum dots: Size-dependent tunable photoluminescence and bioimaging. *New J. Chem.* **2015**, *39*, 8492–8497. [CrossRef]

97. Tuxen, A.; Kibsgaard, J.; Gobel, H.; Laegsgaard, E.; Topsoe, H.; Lauritsen, J.V.; Besenbacher, F. Size Threshold in the Dibenzothiophene Adsorption on MoS_2 Nanoclusters. *Acs Nano* **2010**, *4*, 4677–4682. [CrossRef]

98. Mukundan, A.; Tsao, Y.M.; Artemkina, S.B.; Fedorov, V.E.; Wang, H.C. Growth Mechanism of Periodic-Structured MoS_2 by Transmission Electron Microscopy. *Nanomaterials* **2022**, *12*, 135. [CrossRef]

99. Wu, J.J.; Shen, X.P.; Miao, X.L.; Ji, Z.Y.; Wang, J.H.; Wang, T.; Liu, M.M. An All-Solid-State Z-Scheme g-C_3N_4/Ag/Ag_3VO_4 Photocatalyst with Enhanced Visible-Light Photocatalytic Performance. *Eur. J. Inorg. Chem.* **2017**, *2017*, 2845–2853. [CrossRef]

100. Vinita; Nirala, N.R.; Prakash, R. One step synthesis of AuNPs@MoS_2-QDs composite as a robust peroxidase- mimetic for instant unaided eye detection of glucose inserum, saliva and tear. *Sens. Actuators B Chem.* **2018**, *263*, 109–119. [CrossRef]

101. Lei, L.; Huang, D.L.; Zeng, G.M.; Cheng, M.; Jiang, D.N.; Zhou, C.Y.; Chen, S.; Wang, W.J. A fantastic two-dimensional MoS_2 material based on the inert basal planes activation: Electronic structure, synthesis strategies, catalytic active sites, catalytic and electronics properties. *Coord. Chem. Rev.* **2019**, *399*, 213020. [CrossRef]

102. Huang, J.W.; He, Y.Q.; Jin, J.; Li, Y.R.; Dong, Z.P.; Li, R. A novel glucose sensor based on MoS$_2$ nanosheet functionalized with Ni nanoparticles. *Electrochim. Acta* **2014**, *136*, 41–46. [CrossRef]

103. Huang, K.J.; Liu, Y.J.; Wang, H.B.; Wang, Y.Y.; Liu, Y.M. Sub-femtomolar DNA detection based on layered molybdenum disulfide/multi-walled carbon nanotube composites, Au nanoparticle and enzyme multiple signal amplification. *Biosens. Bioelectron.* **2014**, *55*, 195–202. [CrossRef] [PubMed]

104. Wang, X.; Chu, C.C.; Shen, L.; Deng, W.P.; Yan, M.; Ge, S.G.; Yu, J.H.; Song, X.R. An ultrasensitive electrochemical immunosensor based on the catalytical activity of MoS$_2$-Au composite using Ag nanospheres as labels. *Sens. Actuators B Chem.* **2015**, *206*, 30–36. [CrossRef]

105. Yagati, A.K.; Go, A.; Vu, N.H.; Lee, M.H. A MOS$_2$-Au nanoparticle-modified immunosensor for T-3 biomarker detection in clinical serum samples. *Electrochim. Acta* **2020**, *342*, 136065. [CrossRef]

106. Facure, M.H.M.; Schneider, R.; dos Santos, D.M.; Correa, D.S. Impedimetric electronic tongue based on molybdenum disulfide and graphene oxide for monitoring antibiotics in liquid media. *Talanta* **2020**, *217*, 121039. [CrossRef] [PubMed]

107. Zhao, Y.A.; Zhou, J.; Jia, Z.M.; Huo, D.Q.; Liu, Q.Y.; Zhong, D.Q.; Hu, Y.; Yang, M.; Bian, M.H.; Hou, C.J. In-situ growth of gold nanoparticles on a 3D-network consisting of a MoS$_2$/rGO nanocomposite for simultaneous voltammetric determination of ascorbic acid, dopamine and uric acid. *Microchim. Acta* **2019**, *186*, 92. [CrossRef]

108. Xing, L.W.; Ma, Z.F. A glassy carbon electrode modified with a nanocomposite consisting of MoS$_2$ and reduced graphene oxide for electrochemical simultaneous determination of ascorbic acid, dopamine, and uric acid. *Microchim. Acta* **2016**, *183*, 257–263. [CrossRef]

109. Yang, Y.C.; Qiu, X.J.; Shi, W.; Hou, H.S.; Zou, G.Q.; Huang, W.; Wang, Z.Y.; Leng, S.L.; Ran, Y.Z.; Ji, X.B. Controllable fabrication of two-dimensional layered transition metal oxides through electrochemical exfoliation of non-van der Waals metals for rechargeable zinc-ion batteries. *Chem. Eng. J.* **2021**, *408*, 127247. [CrossRef]

110. Jin, H.Y.; Guo, C.X.; Liu, X.; Liu, J.L.; Vasileff, A.; Jiao, Y.; Zheng, Y.; Qiao, S.Z. Emerging Two-Dimensional Nanomaterials for Electrocatalysis. *Chem. Rev.* **2018**, *118*, 6337–6408. [CrossRef]

111. Kalantar-zadeh, K.; Ou, J.Z.; Daeneke, T.; Mitchell, A.; Sasaki, T.; Fuhrer, M.S. Two dimensional and layered transition metal oxides. *Appl. Mater. Today* **2016**, *5*, 73–89. [CrossRef]

112. Wei, Z.H.; Zhuiykov, S. Challenges and recent advancements of functionalization of two-dimensional nanostructured molybdenum trioxide and dichalcogenides. *Nanoscale* **2019**, *11*, 15709–15738. [CrossRef] [PubMed]

113. Ten Elshof, J.E.; Yuan, H.Y.; Rodriguez, P.G. Two-Dimensional Metal Oxide and Metal Hydroxide Nanosheets: Synthesis, Controlled Assembly and Applications in Energy Conversion and Storage. *Adv. Energy Mater.* **2016**, *6*, 1600355. [CrossRef]

114. Mannhart, J.; Schlom, D.G. Oxide Interfaces-An Opportunity for Electronics. *Science* **2010**, *327*, 1607–1611. [CrossRef]

115. Campbell, C.T.; Sauer, J. Introduction: Surface Chemistry of Oxides. *Chem. Rev.* **2013**, *113*, 3859–3862. [CrossRef]

116. Pacchioni, G.; Freund, H. Electron Transfer at Oxide Surfaces. The MgO Paradigm: From Defects to Ultrathin Films. *Chem. Rev.* **2013**, *113*, 4035–4072. [CrossRef]

117. Helander, M.G.; Wang, Z.B.; Qiu, J.; Lu, Z.H. Band alignment at metal/organic and metal/oxide/organic interfaces. *Appl. Phys. Lett.* **2008**, *93*, 193310. [CrossRef]

118. Menetrey, M.; Markovits, A.; Minot, C. Adsorption of chlorine and oxygen atoms on clean and defective rutile-TiO$_2$ (110) and MgO (100) surfaces. *J. Mol. Struct.* **2007**, *808*, 71–79. [CrossRef]

119. Comini, E.; Sberveglieri, G. Metal oxide nanowires as chemical sensors. *Mater. Today* **2010**, *13*, 28–36. [CrossRef]

120. Sun, Y.F.; Liu, S.B.; Meng, F.L.; Liu, J.Y.; Jin, Z.; Kong, L.T.; Liu, J.H. Metal Oxide Nanostructures and Their Gas Sensing Properties: A Review. *Sensors* **2012**, *12*, 2610–2631. [CrossRef]

121. Gardon, M.; Guilemany, J.M. A review on fabrication, sensing mechanisms and performance of metal oxide gas sensors. *J. Mater. Sci. Mater. Electron.* **2013**, *24*, 1410–1421. [CrossRef]

122. Gao, X.M.; Ouyang, Q.Y.; Zhu, C.L.; Zhang, X.T.; Chen, Y. Porous MoO$_3$/SnO$_2$ Nanoflakes with n-n Junctions for Sensing H$_2$S. *ACS Appl. Nano Mater.* **2019**, *2*, 2418–2425. [CrossRef]

123. Yin, L.; Chen, D.L.; Feng, M.J.; Ge, L.F.; Yang, D.W.; Song, Z.H.; Fan, B.B.; Zhang, R.; Shao, G.S. Hierarchical Fe$_2$O$_3$@WO$_3$ nanostructures with ultrahigh specific surface areas: Microwave-assisted synthesis and enhanced H$_2$S-sensing performance. *RSC Adv.* **2015**, *5*, 328–337. [CrossRef]

124. Li, T.; Yin, W.; Gao, S.W.; Sun, Y.N.; Xu, P.L.; Wu, S.H.; Kong, H.; Yang, G.Z.; Wei, G. The Combination of Two-Dimensional Nanomaterials with Metal Oxide Nanoparticles for Gas Sensors: A Review. *Nanomaterials* **2022**, *12*, 982. [CrossRef] [PubMed]

125. Xu, P.L.; Cui, L.G.; Gao, S.W.; Na, N.; Ebadi, A.G. A theoretical study on sensing properties of in-doped ZnO nanosheet toward acetylene. *Mol. Phys.* **2022**, *120*, e2001957. [CrossRef]

126. Zhou, Q.; Zeng, W.; Chen, W.; Xu, L.; Kumar, R.; Umar, A. High sensitive and low concentration sulfur dioxide (SO$_2$) gas sensor application of heterostructure NiO–ZnO nanodisks. *Sens. Actuators B Chem.* **2019**, *298*, 126870. [CrossRef]

127. Mashtalir, O.; Naguib, M.; Mochalin, V.N.; Dall'Agnese, Y.; Heon, M.; Barsoum, M.W.; Gogotsi, Y. Intercalation and delamination of layered carbides and carbonitrides. *Nat. Commun.* **2013**, *4*, 1716. [CrossRef]

128. Lukatskaya, M.R.; Mashtalir, O.; Ren, C.E.; Dall'Agnese, Y.; Rozier, P.; Taberna, P.L.; Naguib, M.; Simon, P.; Barsoum, M.W.; Gogotsi, Y. Cation Intercalation and High Volumetric Capacitance of Two-Dimensional Titanium Carbide. *Science* **2013**, *341*, 1502–1505. [CrossRef]

129. Khazaei, M.; Arai, M.; Sasaki, T.; Chung, C.Y.; Venkataramanan, N.S.; Estili, M.; Sakka, Y.; Kawazoe, Y. Novel Electronic and Magnetic Properties of Two-Dimensional Transition Metal Carbides and Nitrides. *Adv. Funct. Mater.* **2013**, *23*, 2185–2192. [CrossRef]

130. Naguib, M.; Kurtoglu, M.; Presser, V.; Lu, J.; Niu, J.J.; Heon, M.; Hultman, L.; Gogotsi, Y.; Barsoum, M.W. Two-Dimensional Nanocrystals Produced by Exfoliation of Ti$_3$AlC$_2$. *Adv. Mater.* **2011**, *23*, 4248–4253. [CrossRef]

131. Peng, Q.M.; Guo, J.X.; Zhang, Q.R.; Xiang, J.Y.; Liu, B.Z.; Zhou, A.G.; Liu, R.P.; Tian, Y.J. Unique Lead Adsorption Behavior of Activated Hydroxyl Group in Two-Dimensional Titanium Carbide. *J. Am. Chem. Soc.* **2014**, *136*, 4113–4116. [CrossRef] [PubMed]

132. Ghidiu, M.; Lukatskaya, M.R.; Zhao, M.Q.; Gogotsi, Y.; Barsoum, M.W. Conductive two-dimensional titanium carbide 'clay' with high volumetric capacitance. *Nature* **2014**, *516*, 78–81. [CrossRef] [PubMed]

133. Mashtalir, O.; Naguib, M.; Dyatkin, B.; Gogotsi, Y.; Barsoum, M.W. Kinetics of aluminum extraction from Ti$_3$AlC$_2$ in hydrofluoric acid. *Mater. Chem. Phys.* **2013**, *139*, 147–152. [CrossRef]

134. Barsoum, M.W.; El-Raghy, T. The MAX phases: Unique new carbide and nitride materials—Ternary ceramics turn out to be surprisingly soft and machinable, yet also heat-tolerant, strong and lightweight. *Am. Sci.* **2001**, *89*, 334–343. [CrossRef]

135. Naguib, M.; Mochalin, V.N.; Barsoum, M.W.; Gogotsi, Y. 25th Anniversary Article: MXenes: A New Family of Two-Dimensional Materials. *Adv. Mater.* **2014**, *26*, 992–1005. [CrossRef]

136. Naguib, M.; Halim, J.; Lu, J.; Cook, K.M.; Hultman, L.; Gogotsi, Y.; Barsoum, M.W. New Two-Dimensional Niobium and Vanadium Carbides as Promising Materials for Li-Ion Batteries. *J. Am. Chem. Soc.* **2013**, *135*, 15966–15969. [CrossRef]

137. Ghidiu, M.; Naguib, M.; Shi, C.; Mashtalir, O.; Pan, L.M.; Zhang, B.; Yang, J.; Gogotsi, Y.; Billinge, S.J.L.; Barsoum, M.W. Synthesis and characterization of two-dimensional Nb$_4$C$_3$ (MXene). *Chem. Commun.* **2014**, *50*, 9517–9520. [CrossRef]

138. Enyashin, A.N.; Ivanoyskii, A.L. Structural and Electronic Properties and Stability of MXenes Ti$_2$C and Ti$_3$C$_2$ Functionalized by Methoxy Groups. *J. Phys. Chem. C* **2013**, *117*, 13637–13643. [CrossRef]

139. Xie, Y.; Kent, P.R.C. Hybrid density functional study of structural and electronic properties of functionalized Ti$_{n+1}$X$_n$ (X = C, N) monolayers. *Phys. Rev. B* **2013**, *87*, 235441. [CrossRef]

140. Kurtoglu, M.; Naguib, M.; Gogotsi, Y.; Barsoum, M.W. First principles study of two-dimensional early transition metal carbides. *Mrs Commun.* **2012**, *2*, 133–137. [CrossRef]

141. Mauchamp, V.; Bugnet, M.; Bellido, E.P.; Botton, G.A.; Moreau, P.; Magne, D.; Naguib, M.; Cabioc'h, T.; Barsoum, M.W. Enhanced and tunable surface plasmons in two-dimensional Ti$_3$C$_2$ stacks: Electronic structure versus boundary effects. *Phys. Rev. B* **2014**, *89*, 235428. [CrossRef]

142. Pellegrini, G.; Baldassare, L.; Giliberti, V.; Frigerio, J.; Gallacher, K.; Pau, D.J.; Isella, G.; Ortolani, M.; Biagioni, P. Benchmarking the Use of Heavily Doped Ge for Plasmonics and Sensing in the Mid-Infrared. *Acs Photonics* **2018**, *5*, 3601–3607. [CrossRef]

143. Zhang, H. Ultrathin Two-Dimensional Nanomaterials. *Acs Nano* **2015**, *9*, 9451–9469. [CrossRef] [PubMed]

144. He, L.D.; Wu, J.; Zhu, Y.Z.; Wang, Y.M.; Mei, Y. Covalent Immobilization of Black Phosphorus Quantum Dots on MXene for Enhanced Electrocatalytic Nitrogen Reduction. *Ind. Eng. Chem. Res.* **2021**, *60*, 5443–5450. [CrossRef]

145. Wang, F.; Yang, C.H.; Duan, M.; Tang, Y.; Zhu, J.F. TiO$_2$ nanoparticle modified organ-like Ti$_3$C$_2$ MXene nanocomposite encapsulating hemoglobin for a mediator-free biosensor with excellent performances. *Biosens. Bioelectron.* **2015**, *74*, 1022–1028. [CrossRef]

146. Gusmao, R.; Sofer, Z.; Pumera, M. Black Phosphorus Rediscovered: From Bulk Material to Monolayers. *Angew. Chem. Int. Ed.* **2017**, *56*, 8052–8072. [CrossRef]

147. You, Y.; Goncalves, P.A.D.; Shen, L.F.; Wubs, M.; Deng, X.H.; Xiao, S.S. Magnetoplasmons in monolayer black phosphorus structures. *Opt. Lett.* **2019**, *44*, 554–557. [CrossRef]

148. Zhang, C.D.; Lian, J.C.; Yi, W.; Jiang, Y.H.; Liu, L.W.; Hu, H.; Xiao, W.D.; Du, S.X.; Sun, L.L.; Gao, H.J. Surface Structures of Black Phosphorus Investigated with Scanning Tunneling Microscopy. *J. Phys. Chem. C* **2009**, *113*, 18823–18826. [CrossRef]

149. Kou, L.Z.; Chen, C.F.; Smith, S.C. Phosphorene: Fabrication, Properties, and Applications. *J. Phys. Chem. Lett.* **2015**, *6*, 2794–2805. [CrossRef]

150. Brent, J.R.; Savjani, N.; Lewis, E.A.; Haigh, S.J.; Lewis, D.J.; O'Brien, P. Production of few-layer phosphorene by liquid exfoliation of black phosphorus. *Chem. Commun.* **2014**, *50*, 13338–13341. [CrossRef]

151. Castellanos-Gomez, A.; Vicarelli, L.; Prada, E.; Island, J.O.; Narasimha-Acharya, K.L.; Blanter, S.I.; Groenendijk, D.J.; Buscema, M.; Steele, G.A.; Alvarez, J.V.; et al. Isolation and characterization of few-layer black phosphorus. *2D Mater.* **2014**, *1*, 025001. [CrossRef]

152. Zhao, W.C.; Xue, Z.M.; Wang, J.F.; Jiang, J.Y.; Zhao, X.H.; Mu, T.C. Large-Scale, Highly Efficient, and Green Liquid-Exfoliation of Black Phosphorus in Ionic Liquids. *ACS Appl. Mater. Interfaces* **2015**, *7*, 27608–27612. [CrossRef] [PubMed]

153. Yan, S.C.; Wang, B.J.; Wang, Z.L.; Hu, D.; Xu, X.; Wang, J.Z.; Shi, Y. Supercritical carbon dioxide-assisted rapid synthesis of few-layer black phosphorus for hydrogen peroxide sensing. *Biosens. Bioelectron.* **2016**, *80*, 34–38. [CrossRef]

154. Chen, Y.T.; Ren, R.; Pu, H.H.; Chang, J.B.; Mao, S.; Chen, J.H. Field-effect transistor biosensors with two-dimensional black phosphorus nanosheets. *Biosens. Bioelectron.* **2017**, *89*, 505–510. [CrossRef] [PubMed]

155. Praus, P. A brief review of s-triazine graphitic carbon nitride. *Carbon Lett.* **2022**, *32*, 703–712. [CrossRef]

156. Zhao, G.; Li, W.C.; Zhang, H.Y.; Wang, W.; Ren, Y.P. Single atom Fe-dispersed graphitic carbon nitride (g-C$_3$N$_4$) as a highly efficient peroxymonosulfate photocatalytic activator for sulfamethoxazole degradation. *Chem. Eng. J.* **2022**, *430*, 132937. [CrossRef]

157. Shcherban, N.D.; Diyuk, O.A.; Zazhigalov, V.A.; Murzin, D.Y. Graphitic Carbon Nitride as a Sustainable Catalyst for Selective Ethanol Oxidation. *ACS Sustain. Chem. Eng.* **2021**, *9*, 5128–5137. [CrossRef]

158. Algara-Siller, G.; Severin, N.; Chong, S.Y.; Bjorkman, T.; Palgrave, R.G.; Laybourn, A.; Antonietti, M.; Khimyak, Y.Z.; Krasheninnikov, A.V.; Rabe, J.P.; et al. Triazine-Based Graphitic Carbon Nitride: A Two-Dimensional Semiconductor. *Angew. Chem. Int. Ed.* **2014**, *53*, 7450–7455. [CrossRef]
159. Tang, Y.R.; Song, H.J.; Su, Y.Y.; Lv, Y. Turn-on Persistent Luminescence Probe Based on Graphitic Carbon Nitride for Imaging Detection of Biothiols in Biological Fluids. *Anal. Chem.* **2013**, *85*, 11876–11884. [CrossRef]
160. Zhang, G.G.; Zhang, M.W.; Ye, X.X.; Qiu, X.Q.; Lin, S.; Wang, X.C. Iodine Modified Carbon Nitride Semiconductors as Visible Light Photocatalysts for Hydrogen Evolution. *Adv. Mater.* **2014**, *26*, 805–809. [CrossRef]
161. Yang, S.B.; Gong, Y.J.; Zhang, J.S.; Zhan, L.; Ma, L.L.; Fang, Z.Y.; Vajtai, R.; Wang, X.C.; Ajayan, P.M. Exfoliated Graphitic Carbon Nitride Nanosheets as Efficient Catalysts for Hydrogen Evolution Under Visible Light. *Adv. Mater.* **2013**, *25*, 2452–2456. [CrossRef] [PubMed]
162. Zhu, J.J.; Xiao, P.; Li, H.L.; Carabineiro, S.A.C. Graphitic Carbon Nitride: Synthesis, Properties, and Applications in Catalysis. *ACS Appl. Mater. Interfaces* **2014**, *6*, 16449–16465. [CrossRef] [PubMed]
163. Zhang, K.L.; Feng, Y.L.; Wang, F.; Yang, Z.C.; Wang, J. Two dimensional hexagonal boron nitride (2D-hBN): Synthesis, properties and applications. *J. Mater. Chem. C* **2017**, *5*, 11992–12022. [CrossRef]
164. Topsakal, M.; Akturk, E.; Ciraci, S. First-principles study of two- and one-dimensional honeycomb structures of boron nitride. *Phys. Rev. B* **2009**, *79*, 115442. [CrossRef]
165. Sajjad, M.; Feng, P. Study the gas sensing properties of boron nitride nanosheets. *Mater. Res. Bull.* **2014**, *49*, 35–38. [CrossRef]
166. Li, L.H.; Chen, Y. Atomically Thin Boron Nitride: Unique Properties and Applications. *Adv. Funct. Mater.* **2016**, *26*, 2594–2608. [CrossRef]
167. Weng, Q.H.; Wang, X.B.; Wang, X.; Bando, Y.; Golberg, D. Functionalized hexagonal boron nitride nanomaterials: Emerging properties and applications. *Chem. Soc. Rev.* **2016**, *45*, 3989–4012. [CrossRef]
168. Ma, S.X.; Li, D.J.; Rao, X.J.; Xia, X.F.; Su, Y.; Lu, Y.F. Pd-doped h-BN monolayer: A promising gas scavenger for SF6 insulation devices. *Adsorption* **2020**, *26*, 619–626. [CrossRef]
169. Yamini, Y.; Moradi, M. Influence of topological defects on the nitrogen monoxide-sensing characteristics of graphene-analogue BN. *Sens. Actuators B Chem.* **2014**, *197*, 274–279. [CrossRef]
170. Xu, P.L.; Cao, J.Y.; Yin, C.; Wang, L.T.; Wu, L. Quantum chemical study on the adsorption of megazol drug on the pristine BC_3 nanosheet. *Supramol. Chem.* **2021**, *33*, 63–69. [CrossRef]
171. Calabrese, E.J.; Bachmann, K.A.; Bailer, A.J.; Bolger, P.M.; Borak, J.; Cai, L.; Cedergreen, N.; Cherian, M.G.; Chiueh, C.C.; Clarkson, T.W.; et al. Biological stress response terminology: Integrating the concepts of adaptive response and preconditioning stress within a hormetic dose-response framework. *Toxicol. Appl. Pharmacol.* **2007**, *222*, 122–128. [CrossRef] [PubMed]
172. Li, X.J.; Ping, J.F.; Ying, Y.B. Recent developments in carbon nanomaterial-enabled electrochemical sensors for nitrite detection. *Trends Analyt. Chem.* **2019**, *113*, 1–12. [CrossRef]
173. Han, Z.; Tang, Z.M.; Jiang, K.Q.; Huang, Q.W.; Meng, J.J.; Nie, D.X.; Zhao, Z.H. Dual-target electrochemical aptasensor based on co-reduced molybdenum disulfide and Au NPs (rMoS(2)-Au) for multiplex detection of mycotoxins. *Biosens. Bioelectron.* **2020**, *150*, 111894. [CrossRef] [PubMed]
174. Sookhakian, M.; Basirun, W.J.; Goh, B.T.; Woi, P.M.; Alias, Y. Molybdenum disulfide nanosheet decorated with silver nanoparticles for selective detection of dopamine. *Colloids Surf. B* **2019**, *176*, 80–86. [CrossRef] [PubMed]
175. Chen, L.; Ji, L.F.; Zhao, J.; Zhang, X.; Yang, F.C.; Liu, J.T. Facile exfoliation of molybdenum disulfide nanosheets as highly efficient electrocatalyst for detection of m-nitrophenol. *J. Electroanal. Chem.* **2017**, *801*, 300–305. [CrossRef]
176. Zhang, S.; Tang, Y.P.; Chen, Y.Y.; Zheng, J.B. Synthesis of gold nanoparticles coated on flower-like MoS_2 microsphere and their application for electrochemical nitrite sensing. *J. Electroanal. Chem.* **2019**, *839*, 195–201. [CrossRef]
177. Yang, Y.; Zhang, J.; Li, Y.W.; Shan, Q.; Wu, W. Ni nanosheets evenly distributed on MoS_2 for selective electrochemical detection of nitrite. *Colloid Surf. A* **2021**, *625*, 126865. [CrossRef]
178. Haldorai, Y.; Kim, J.Y.; Vilian, A.T.E.; Heo, N.S.; Huh, Y.S.; Han, Y.K. An enzyme-free electrochemical sensor based on reduced graphene oxide/Co_3O_4 nanospindle composite for sensitive detection of nitrite. *Sens. Actuators B Chem.* **2016**, *227*, 92–99. [CrossRef]
179. Zhang, Y.; Chen, P.; Wen, F.F.; Yuan, B.; Wang, H.G. Fe_3O_4 nanospheres on MoS_2 nanoflake: Electrocatalysis and detection of Cr(VI) and nitrite. *J. Electroanal. Chem.* **2016**, *761*, 14–20. [CrossRef]
180. Baumgartner, T.; Huynh, K.; Schleidt, S.; Lough, A.J.; Manners, I. Metallochain cluster complexes and metallomacrocyclic triangles based on coordination bonds between palladium or platinum and diphosphinoacetylene ligands. *Chem. Eur. J.* **2002**, *8*, 4622–4632. [CrossRef]
181. Gumpu, M.B.; Sethuraman, S.; Krishnan, U.M.; Rayappan, J.B.B. A review on detection of heavy metal ions in water—An electrochemical approach. *Sens. Actuators B Chem.* **2015**, *213*, 515–533. [CrossRef]
182. Zhou, W.S.; Li, C.H.; Sun, C.; Yang, X.D. Simultaneously determination of trace Cd^{2+} and Pb^{2+} based on L-cysteine/graphene modified glassy carbon electrode. *Food Chem.* **2016**, *192*, 351–357. [CrossRef] [PubMed]
183. Zhu, X.L.; Liu, B.C.; Hou, H.J.; Huang, Z.Y.; Zeinu, K.M.; Huang, L.; Yuan, X.Q.; Guo, D.B.; Hu, J.P.; Yang, J.K. Alkaline intercalation of Ti_3C_2 MXene for simultaneous electrochemical detection of Cd(II), Pb(II), Cu(II) and Hg(II). *Electrochim. Acta* **2017**, *248*, 46–57. [CrossRef]

184. Mahmoudian, M.R.; Alias, Y.; Basirun, W.J.; Woi, P.M.; Sookhakian, M.; Jamali-Sheini, F. Synthesis and characterization of Fe_3O_4 rose like and spherical/reduced graphene oxide nanosheet composites for lead (II) sensor. *Electrochim. Acta* **2015**, *169*, 126–133. [CrossRef]

185. Tan, F.; Cong, L.C.; Saucedo, N.M.; Gao, J.S.; Li, X.N.; Mulchandani, A. An electrochemically reduced graphene oxide chemiresistive sensor for sensitive detection of Hg^{2+} ion in water samples. *J. Hazard. Mater.* **2016**, *320*, 226–233. [CrossRef]

186. Rahman, M.T.; Kabir, M.F.; Gurung, A.; Reza, K.M.; Pathak, R.; Ghimire, N.; Baride, A.; Wang, Z.Q.; Kurnar, M.; Qiao, Q.Q. Graphene Oxide-Silver Nanowire Nanocomposites for Enhanced Sensing of Hg^{2+}. *ACS Appl. Nano Mater.* **2019**, *2*, 4842–4851. [CrossRef]

187. Wei, Y.; Gao, C.; Meng, F.L.; Li, H.H.; Wang, L.; Liu, J.H.; Huang, X.J. SnO_2/Reduced Graphene Oxide Nanocomposite for the Simultaneous Electrochemical Detection of Cadmium(II), Lead(II), Copper(II), and Mercury(II): An Interesting Favorable Mutual Interference. *J. Phys. Chem. C* **2012**, *116*, 1034–1041. [CrossRef]

188. Sun, H.Y.; Wang, C.X.; Xu, Y.J.; Dai, D.M.; Deng, X.Y.; Gao, H.T. A Novel Electrochemical Sensor Based on A Glassy Carbon Electrode Modified with GO/MnO_2 for Simultaneous Determination of Trace Cu(II) and Pb(II) in Environmental Water. *Chemistryselect* **2019**, *4*, 11862–11871. [CrossRef]

189. Jiang, R.Y.; Liu, N.T.; Su, Y.H.; Gao, S.S.; Mamat, X.; Wagberg, T.; Li, Y.T.; Hu, X.; Hu, G.Z. Polysulfide/Graphene Nanocomposite Film for Simultaneous Electrochemical Determination of Cadmium and Lead Ions. *Nano* **2018**, *13*, 1850090. [CrossRef]

190. Barton, M.D. Antibiotic use in animal feed and its impact on human health. *Nutr. Res. Rev.* **2000**, *13*, 279–299. [CrossRef]

191. Jiao, Y.C.; Hou, W.J.; Fu, J.Y.; Guo, Y.M.; Xia, S.; Wang, X.Y.; Jing, Z. A nanostructured electrochemical aptasensor for highly sensitive detection of chlorpyrifos. *Sens. Actuators B Chem.* **2017**, *243*, 1164–1170. [CrossRef]

192. Zhou, Q.; Yang, L.; Wang, G.C.; Yang, Y. Acetylcholinesterase biosensor based on SnO_2 nanoparticles-carboxylic graphene-nafion modified electrode for detection of pesticides. *Biosens. Bioelectron.* **2013**, *49*, 25–31. [CrossRef] [PubMed]

193. Kokulnathan, T.; Vishnuraj, R.; Wang, T.J.; Kumar, E.A.; Pullithadathil, B. Heterostructured bismuth oxide/hexagonal-boron nitride nanocomposite: A disposable electrochemical sensor for detection of flutamide. *Ecotoxicol. Environ. Saf.* **2021**, *207*, 111276. [CrossRef] [PubMed]

194. Li, Z.; Jiang, S.Z.; Huo, Y.Y.; Ning, T.Y.; Liu, A.H.; Zhang, C.; He, Y.; Wang, M.H.; Li, C.H.; Man, B.Y. 3D silver nanoparticles with multilayer graphene oxide as a spacer for surface enhanced Raman spectroscopy analysis. *Nanoscale* **2018**, *10*, 5897–5905. [CrossRef]

195. Nasir, M.Z.M.; Mayorga-Martinez, C.C.; Sofer, Z.; Pumera, M. Two-Dimensional 1T-Phase Transition Metal Dichalcogenides as Nanocarriers to Enhance and Stabilize Enzyme Activity for Electrochemical Pesticide Detection. *Acs Nano* **2017**, *11*, 5774–5784. [CrossRef]

196. Song, D.D.; Li, Q.; Lu, X.; Li, Y.S.; Li, Y.; Wang, Y.Z.; Gao, F.M. Ultra-thin bimetallic alloy nanowires with porous architecture/monolayer MoS_2 nanosheet as a highly sensitive platform for the electrochemical assay of hazardous omethoate pollutant. *J. Hazard. Mater.* **2018**, *357*, 466–474. [CrossRef]

197. Song, D.D.; Wang, Y.Z.; Lu, X.; Gao, Y.K.; Li, Y.; Gao, F.M. Ag nanoparticles-decorated nitrogen-fluorine co-doped monolayer MoS_2 nanosheet for highly sensitive electrochemical sensing of organophosphorus pesticides. *Sens. Actuators B Chem.* **2018**, *267*, 5–13. [CrossRef]

198. Jiang, Y.J.; Zhang, X.N.; Pei, L.J.; Yue, S.; Ma, L.; Zhou, L.Y.; Huang, Z.H.; He, Y.; Gao, J. Silver nanoparticles modified two-dimensional transition metal carbides as nanocarriers to fabricate acetycholinesterase-based electrochemical biosensor. *Chem. Eng. J.* **2018**, *339*, 547–556. [CrossRef]

199. Peng, Y.; Tang, Z.R.; Dong, Y.P.; Che, G.; Xin, Z.F. Electrochemical detection of hydroquinone based on MoS_2/reduced graphene oxide nanocomposites. *J. Electroanal. Chem.* **2018**, *816*, 38–44. [CrossRef]

200. Wu, L.X.; Lu, X.B.; Dhanjai; Wu, Z.S.; Dong, Y.F.; Wang, X.H.; Zheng, S.H.; Chen, J.P. 2D transition metal carbide MXene as a robust biosensing platform for enzyme immobilization and ultrasensitive detection of phenol. *Biosens. Bioelectron.* **2018**, *107*, 69–75. [CrossRef]

201. Luong, J.H.T.; Male, K.B.; Glennon, J.D. Biosensor technology: Technology push versus market pull. *Biotechnol. Adv.* **2008**, *26*, 492–500. [CrossRef] [PubMed]

202. Andreescu, S.; Sadik, O.A. Trends and challenges in biochemical sensors for clinical and environmental monitoring. *Pure Appl. Chem.* **2004**, *76*, 861–878. [CrossRef]

203. Liu, B.; Jiang, M.; Zhu, D.Z.; Zhang, J.M.; Wei, G. Metal-organic frameworks functionalized with nucleic acids and amino acids for structure- and function-specific applications: A tutorial review. *Chem. Eng. J.* **2022**, *428*, 131118. [CrossRef]

204. Shavanova, K.; Bakakina, Y.; Burkova, I.; Shtepliuk, I.; Viter, R.; Ubelis, A.; Beni, V.; Starodub, N.; Yakimova, R.; Khranovskyy, V. Application of 2D Non-Graphene Materials and 2D Oxide Nanostructures for Biosensing Technology. *Sensors* **2016**, *16*, 223. [CrossRef] [PubMed]

205. Su, S.; Zhang, C.; Yuwen, L.H.; Liu, X.F.; Wang, L.H.; Fan, C.H.; Wang, L.H. Uniform Au@Pt core-shell nanodendrites supported on molybdenum disulfide nanosheets for the methanol oxidation reaction. *Nanoscale* **2016**, *8*, 602–608. [CrossRef]

206. Zhang, Y.F.; Bo, X.J.; Nsabimana, A.; Luhana, C.; Wang, G.; Wang, H.; Li, M.; Guo, L.P. Fabrication of 2D ordered mesoporous carbon nitride and its use as electrochemical sensing platform for H_2O_2, nitrobenzene, and NADH detection. *Biosens. Bioelectron.* **2014**, *53*, 250–256. [CrossRef]

207. Wu, S.X.; Zeng, Z.Y.; He, Q.Y.; Wang, Z.J.; Wang, S.J.; Du, Y.P.; Yin, Z.Y.; Sun, X.P.; Chen, W.; Zhang, H. Electrochemically Reduced Single-Layer MoS$_2$ Nanosheets: Characterization, Properties, and Sensing Applications. *Small* **2012**, *8*, 2264–2270. [CrossRef]

208. Song, Y.H.; Wei, C.T.; He, J.; Li, X.; Lu, X.P.; Wang, L. Porous Co nanobeads/rGO nanocomposites derived from rGO/Co-metal organic frameworks for glucose sensing. *Sens. Actuators B Chem.* **2015**, *220*, 1056–1063. [CrossRef]

209. Parlak, O.; Incel, A.; Uzun, L.; Turner, A.P.F.; Tiwari, A. Structuring Au nanoparticles on two-dimensional MoS$_2$ nanosheets for electrochemical glucose biosensors. *Biosens. Bioelectron.* **2017**, *89*, 545–550. [CrossRef]

210. Kavitha, T.; Gopalan, A.I.; Lee, K.P.; Park, S.Y. Glucose sensing, photocatalytic and antibacterial properties of graphene-ZnO nanoparticle hybrids. *Carbon* **2012**, *50*, 2994–3000. [CrossRef]

211. Liu, M.M.; Liu, R.; Chen, W. Graphene wrapped Cu$_2$O nanocubes: Non-enzymatic electrochemical sensors for the detection of glucose and hydrogen peroxide with enhanced stability. *Biosens. Bioelectron.* **2013**, *45*, 206–212. [CrossRef] [PubMed]

212. Wang, Q.Y.; Cui, X.Q.; Chen, J.L.; Zheng, X.L.; Liu, C.; Xue, T.Y.; Wang, H.T.; Jin, Z.; Qiao, L.; Zheng, W.T. Well-dispersed palladium nanoparticles on graphene oxide as a non-enzymatic glucose sensor. *RSC Adv.* **2012**, *2*, 6245–6249. [CrossRef]

213. Apel, K.; Hirt, H. Reactive oxygen species: Metabolism, oxidative stress, and signal transduction. *Annu. Rev. Plant Biol* **2004**, *55*, 373–399. [CrossRef] [PubMed]

214. Preston, T.J.; Muller, W.J.; Singh, G. Scavenging of extracellular H$_2$O$_2$ by catalase inhibits the proliferation of HER-2/Neu-transformed rat-1 fibroblasts through the induction of a stress response. *J. Biol. Chem.* **2001**, *276*, 9558–9564. [CrossRef] [PubMed]

215. Li, W.H.; Li, M.S.; Yang, Z.Z.; Xu, J.; Zhong, X.W.; Wang, J.Q.; Zeng, L.C.; Liu, X.W.; Jiang, Y.; Wei, X.; et al. Carbon-Coated Germanium Nanowires on Carbon Nanofibers as Self-Supported Electrodes for Flexible Lithium-Ion Batteries. *Small* **2015**, *11*, 2762–2767. [CrossRef] [PubMed]

216. Tian, J.Q.; Liu, Q.; Asiri, A.M.; Qusti, A.H.; Al-Youbi, A.O.; Sun, X.P. Ultrathin graphitic carbon nitride nanosheets: A novel peroxidase mimetic, Fe doping-mediated catalytic performance enhancement and application to rapid, highly sensitive optical detection of glucose. *Nanoscale* **2013**, *5*, 11604–11609. [CrossRef]

217. Saha, K.; Agasti, S.S.; Kim, C.; Li, X.N.; Rotello, V.M. Gold Nanoparticles in Chemical and Biological Sensing. *Chem. Rev.* **2012**, *112*, 2739–2779. [CrossRef]

218. Fritea, L.; Banica, F.; Costea, T.O.; Moldovan, L.; Dobjanschi, L.; Muresan, M.; Cavalu, S. Metal Nanoparticles and Carbon-Based Nanomaterials for Improved Performances of Electrochemical (Bio)Sensors with Biomedical Applications. *Materials* **2021**, *14*, 6319. [CrossRef]

219. Maduraiveeran, G.; Sasidharan, M.; Ganesan, V. Electrochemical sensor and biosensor platforms based on advanced nanomaterials for biological and biomedical applications. *Biosens. Bioelectron.* **2018**, *103*, 113–129. [CrossRef]

220. Sun, H.F.; Chao, J.; Zuo, X.L.; Su, S.; Liu, X.F.; Yuwen, L.H.; Fan, C.H.; Wang, L.H. Gold nanoparticle-decorated MoS$_2$ nanosheets for simultaneous detection of ascorbic acid, dopamine and uric acid. *RSC Adv.* **2014**, *4*, 27625–27629. [CrossRef]

221. Huang, K.J.; Liu, Y.J.; Liu, Y.M.; Wang, L.L. Molybdenum disulfide nanoflower-chitosan-Au nanoparticles composites based electrochemical sensing platform for bisphenol A determination. *J. Hazard. Mater.* **2014**, *276*, 207–215. [CrossRef] [PubMed]

222. Zhang, Y.H.; Zhang, Q.X.; Lu, W. One-step synthesis of graphene/Au nanoparticle composite by epoxy resin: Electrocatalytic detection of H$_2$O$_2$ and catalytic reduction of 4-nitrophenol. *Mater. Res. Express.* **2017**, *4*, 105012. [CrossRef]

223. Shu, Y.; Chen, J.Y.; Xu, Q.; Wei, Z.; Liu, F.P.; Lu, R.; Xu, S.; Hu, X.Y. MoS$_2$ nanosheet-Au nanorod hybrids for highly sensitive amperometric detection of H$_2$O$_2$ in living cells. *J. Mater. Chem. B* **2017**, *5*, 1446–1453. [CrossRef] [PubMed]

224. Su, S.; Han, X.Y.; Lu, Z.W.; Liu, W.; Zhu, D.; Chao, J.; Fan, C.H.; Wang, L.H.; Song, S.P.; Weng, L.X.; et al. Facile Synthesis of a MoS$_2$-Prussian Blue Nanocube Nanohybrid-Based Electrochemical Sensing Platform for Hydrogen Peroxide and Carcinoembryonic Antigen Detection. *ACS Appl. Mater. Interfaces* **2017**, *9*, 12773–12781. [CrossRef]

225. Yang, T.; Meng, L.; Chen, H.Y.; Luo, S.Z.; Li, W.H.; Jiao, K. Synthesis of Thin-Layered Molybdenum Disulfide-Based Polyaniline Nanointerfaces for Enhanced Direct Electrochemical DNA Detection. *Adv. Mater. Interfaces* **2016**, *3*, 1500700. [CrossRef]

226. Chu, Y.L.; Cai, B.; Ma, Y.; Zhao, M.G.; Ye, Z.Z.; Huang, J.Y. Highly sensitive electrochemical detection of circulating tumor DNA based on thin-layer MoS$_2$/graphene composites. *RSC Adv.* **2016**, *6*, 22673–22678. [CrossRef]

227. Xing, Z.C.; Yang, X.R.; Asiri, A.M.; Sun, X.P. Three-Dimensional Structures of MoS$_2$@Ni Core/Shell Nanosheets Array toward Synergetic Electrocatalytic Water Splitting. *ACS Appl. Mater. Interfaces* **2016**, *8*, 14521–14526. [CrossRef]

228. Liu, H.; Chen, X.J.; Su, X.; Duan, C.Y.; Guo, K.; Zhu, Z.F. Flower-like MoS$_2$ Modified Reduced Graphene Oxide Nanocomposite: Synthesis and Application for Lithium-Ion Batteries and Mediator-Free Biosensor. *J. Electrochem. Soc.* **2015**, *162*, B312–B318. [CrossRef]

229. Wang, Y.H.; Ning, G.; Bi, H.; Wu, Y.H.; Liu, G.Q.; Zhao, Y.L. A novel ratiometric electrochemical assay for ochratoxin A coupling Au nanoparticles decorated MoS$_2$ nanosheets with aptamer. *Electrochim. Acta* **2018**, *285*, 120–127. [CrossRef]

230. Jiang, D.; Wei, M.; Du, X.J.; Qin, M.; Shan, X.L.; Chen, Z.D. One-pot synthesis of ZnO quantum dots/N-doped Ti$_3$C$_2$ MXene: Tunable nitrogen-doping properties and efficient electrochemiluminescence sensing. *Chem. Eng. J.* **2022**, *430*, 132771. [CrossRef]

231. Gu, H.; Zhou, T.S.; Shi, G.Y. Synthesis of graphene supported graphene-like C$_3$N$_4$ metal-free layered nanosheets for enhanced electrochemical performance and their biosensing for biomolecules. *Talanta* **2015**, *132*, 871–876. [CrossRef] [PubMed]

232. Wang, T.Y.; Zhu, H.C.; Zhuo, J.Q.; Zhu, Z.W.; Papakonstantinou, P.; Lubarsky, G.; Lin, J.; Li, M.X. Biosensor Based on Ultrasmall MoS$_2$ Nanoparticles for Electrochemical Detection of H$_2$O$_2$ Released by Cells at the Nanomolar Level. *Anal. Chem.* **2013**, *85*, 10289–10295. [CrossRef] [PubMed]

233. Song, H.Y.; Ni, Y.N.; Kokot, S. Investigations of an electrochemical platform based on the layered MoS$_2$-graphene and horseradish peroxidase nanocomposite for direct electrochemistry and electrocatalysis. *Biosens. Bioelectron.* **2014**, *56*, 137–143. [CrossRef]

234. Zhu, L.L.; Zhang, Y.; Xu, P.C.; Wen, W.J.; Li, X.X.; Xu, J.Q. PtW/MoS$_2$ hybrid nanocomposite for electrochemical sensing of H$_2$O$_2$ released from living cells. *Biosens. Bioelectron.* **2016**, *80*, 601–606. [CrossRef]

235. Lin, X.Y.; Ni, Y.N.; Kokot, S. Electrochemical and bio-sensing platform based on a novel 3D Cu nano-flowers/layered MoS$_2$ composite. *Biosens. Bioelectron.* **2016**, *79*, 685–692. [CrossRef]

236. Su, S.; Sun, H.F.; Xu, F.; Yuwen, L.H.; Fan, C.H.; Wang, L.H. Direct electrochemistry of glucose oxidase and a biosensor for glucose based on a glass carbon electrode modified with MoS$_2$ nanosheets decorated with gold nanoparticles. *Microchim. Acta* **2014**, *181*, 1497–1503. [CrossRef]

237. Huang, K.J.; Zhang, J.Z.; Liu, Y.J.; Wang, L.L. Novel electrochemical sensing platform based on molybdenum disulfide nanosheets-polyaniline composites and Au nanoparticles. *Sens. Actuators B Chem.* **2014**, *194*, 303–310. [CrossRef]

238. Su, S.; Sun, H.F.; Xu, F.; Yuwen, L.H.; Wang, L.H. Highly Sensitive and Selective Determination of Dopamine in the Presence of Ascorbic Acid Using Gold Nanoparticles-Decorated MoS$_2$ Nanosheets Modified Electrode. *Electroanalysis* **2013**, *25*, 2523–2529. [CrossRef]

239. Omar, M.N.; Salleh, A.; Lim, H.N.; Tajudin, A.A. Electrochemical detection of uric acid via uricase-immobilized graphene oxide. *Anal. Biochem.* **2016**, *509*, 135–141. [CrossRef]

240. Xia, X.H.; Zheng, Z.X.; Zhang, Y.; Zhao, X.J.; Wang, C.M. Synthesis of Ag-MoS$_2$/chitosan nanocomposite and its application for catalytic oxidation of tryptophan. *Sens. Actuators B Chem.* **2014**, *192*, 42–50. [CrossRef]

241. Yang, R.R.; Zhao, J.L.; Chen, M.J.; Yang, T.; Luo, S.Z.; Jiao, K. Electrocatalytic determination of chloramphenicol based on molybdenum disulfide nanosheets and self-doped polyaniline. *Talanta* **2015**, *131*, 619–623. [CrossRef] [PubMed]

242. Yola, M.L.; Eren, T.; Atar, N. A sensitive molecular imprinted electrochemical sensor based on gold nanoparticles decorated graphene oxide: Application to selective determination of tyrosine in milk. *Sens. Actuators B Chem.* **2015**, *210*, 149–157. [CrossRef]

243. Jiang, L.; Gu, S.Q.; Ding, Y.P.; Ye, D.X.; Zhang, Z.; Zhang, F.F. Amperometric sensor based on tricobalt tetraoxide nanoparticles-graphene nanocomposite film modified glassy carbon electrode for determination of tyrosine. *Colloids Surf. B* **2013**, *107*, 146–151. [CrossRef] [PubMed]

244. Huang, J.L.; Tian, J.N.; Zhao, Y.C.; Zhao, S.L. Ag/Au nanoparticles coated graphene electrochemical sensor for ultrasensitive analysis of carcinoembryonic antigen in clinical immunoassay. *Sens. Actuators B Chem.* **2015**, *206*, 570–576. [CrossRef]